Nonuniform localized distortions in generalized elasticity for liquid crystals

G. De Matteis,[1,2,3,*] L. Martina,[1,2,†] C. Naya,[2,‡] and V. Turco[1,2,3,§]

[1]*Dipartimento di Matematica e Fisica, Università del Salento, Via per Arnesano, C.P. 73100 Lecce, Italy*

[2]*INFN, Sezione di Lecce, Via per Arnesano, C.P. 193, I-73100 Lecce, Italy*

[3]*GNFM-INDAM, Città Universitaria, Piazzale Aldo Moro 5, C.P. 00185 Roma, Italy*

(Received 12 June 2020; accepted 7 October 2020; published 26 October 2020)

We analyze a recent generalized free-energy for liquid crystals posited by Virga and falling in the class of quartic functionals in the spatial gradients of the nematic director. We review some known interesting solutions, i.e., uniform heliconical structures, and we find new liquid crystal configurations, which closely resemble some novel, experimentally detected, structures called Skyrmion tubes. These new configurations are characterized by a localized pattern given by the variation of the conical angle. We study the equilibrium differential equations and find numerical solutions and analytical approximations.

DOI: 10.1103/PhysRevE.102.042705

I. INTRODUCTION

Until recently, uniform nematics, smectics, cholesterics, and blue phases have been known to cover the vast phenomenology observed for liquid crystals [1–4]. All of them show interesting new properties and phase transitions when frustrated by geometric confinement and/or external fields [1–3,5–7]. In particular, in recent years it has been demonstrated that chiral nematics can be host to a plethora of new topological and nontopological solitonic structures, i.e., skyrmions, helicoids, merons, and hopfions [8–13]. Furthermore, skyrmion clusters with mutually orthogonal orientations of the constituent isolated skyrmions have been observed and studied in frustrated chiral liquid crystals [14,15].

On the other hand, a new class of nematics was recently found in bent-core and dimeric systems with clearly recognizable "banana"-like bent-shaped molecules [16,17]. Besides the conventional uniform nematic N phase, these materials can spontaneously form a new one, now recognized as the *twist-bend* nematic phase N_{TB} [18]. Especially surprising is the fact that the observed new phases exhibit helical (chiral) orientational ordering despite being formed from achiral molecules. For comparison, conventional uniaxial nematic liquid crystals (N), which have been known for more than a century, are formed from rodlike or dislike molecules. The chiral cholesteric phases are locally equivalent to nematics but possess simple (orthogonal) helical structures with pitches in the few-micron range: The nematic director $\boldsymbol{n}$ twists in space, drawing a right-angle helicoid and remaining perpendicular to the helix axis. The cholesteric structure appears as a result of relatively weak molecular chirality (that is why there is a relatively large pitch), and the swirl direction of the spiral (left or right) is determined by the sign of the molecular chirality. On the other hand, the action of external fields may induce a deformation of the cholesteric helix into an oblique helicoid with an acute tilt angle [19–23], which is usually theoretically analyzed on the basis of the classical Frank-Oseen theory. Unlike this situation, in the N_{TB} nematics the achiral molecules tend to spontaneously, i.e., with no external fields, arrange in heliconical structures with twist and bend deformations: The molecular axes are tilted from the helical axis by an angle θ_{TB} and the director follows an oblique helicoid. The N_{TB} phase is stabilized below the uniaxial nematic phase N through both first-order or second-order temperature-driven transitions [24], as a result of the spontaneous chiral symmetry breaking. Indeed, a mechanism of this kind is not new to liquid crystal systems (see for instance [25] or [26]). These structures are similar to the smectic SmC^* phases but, at variance with them, the heliconical textures do not possess any layer periodicity. Moreover the helical pitch, experimentally found to be on the order of 10 nm, is much smaller than the standard cholesteric one. Direct observation of the periodic heliconical structure was first achieved by the authors of [16,17] with an estimation of the periodicity around 8 nm. The new twist-bend nematic represents a structural link between the uniaxial nematic phase N, with no tilt, and an unperturbed chiral nematic, i.e., helicoids with right-angle tilt. Although the essential features of the heliconical phase and the N-N_{TB} transitions have been outlined by several experimental studies [27–35], the elastic properties of the N_{TB} phase still remain unknown. Nevertheless, several attempts have been made so far to posit a coherent elastic continuum theory [36–41].

In fact, by scanning the literature, one can find a number of theoretical works devoted to the twist-bend nematics [37,42–45]. Meyer was the first to hypothesize such heliconical structures in the 1970s, proposing that they were originated from a spontaneous appearance of the bend flexoelectric polarization [46]. Later on, the majority of the theoretical works, starting from the influential [42], discuss

*giovanni.dematteis@istruzione.it
†martina@le.infn.it
‡carlos.naya@le.infn.it
§vito.turco@le.infn.it

the question of how modulated orientational structures can be formed in achiral systems. One can easily understand that the description of the twist-bend nematics in terms of an orientational elastic energy requires a pathological (not positively defined) Frank elastic energy. An analysis in the framework of such Frank energy can explain some experimental observations made for the N_{TB} liquid crystals, e.g., anomalously large flexoelectric coefficients [45] or nonmonotonic temperature dependence of the orientational elastic moduli [43]. Moreover, in [26] the negative twist elasticity yielding the spontaneous chiral symmetry breaking, has been suggested based on the van der Waals contribution into the Frank elastic moduli.

In [42] Dozov proposed a first elastic theory by using second-order spatial derivatives of the nematic director field, higher than the first order usually employed in the classical Frank's theory. Dozov's theory departs from Frank's also for the sign of the bend elastic constant K_{33}, which turns negative and, therefore, higher order invariants are needed in the elastic free-energy density in order to stabilize the heliconical state. Moreover in [42], Dozov also provides a qualitative description of two one-dimensional periodic structures by suitably selecting high order invariants. For most liquid crystals problems and applications, it is sufficient to consider just the first derivatives of the director. However, in cases such as the twist-bend phase in bent-core liquid crystals or chromonic liquid crystals, where one of the elastic constants may turn negative, higher order terms may have to be added to the Frank-Oseen free energy density. A particular higher order term has been widely discussed in the literature, also concerning its possible role in the stabilization of the twist-bend phase [47]. The Frank-Oseen energy density functional is sometimes written with an additional surface energy contribution besides the saddle-splay term K_{24}. It is a second-order surface term called splay bend, i.e., $K_{13}\,\mathrm{div}(\boldsymbol{n}\,\mathrm{div}\boldsymbol{n})$, which was first introduced phenomenologically by Oseen [48], neglected by Frank [49], and reintroduced by Nehring and Saupe [50]. On the other hand, this higher-order term may favor configurations with arbitrary large second derivatives, possibly leading to instabilities. Later on, several studies addressed the theoretical analysis of the N_{TB} phase [36,37,45,51]. In particular, in [51] a N-N_{TB} phase transition was described using a generalized Maier-Saupe molecular field theory. In [36], a generalized Landau–de Gennes theory was used to investigate one-dimensional modulated nematic structures generated by nonchiral and intrinsically chiral V-shaped molecules. In [37], the N_{TB} phase was treated as a mixture of two different ordinary N phases, both presenting heliconical structures with the same pitch but opposite helicities. A quadratic elastic theory, still featuring four Frank's elastic constants, was used for each of the two helical phases. Similar models were proposed in [38–40], where also the effects of an external magnetic or electric bulk field were investigated. Again, authors in [52,53] proposed coarse-grained elastic models, which, similarly to the model for SmA^* [1], make use of an extra scalar order parameter. In [38] N_{TB} phase elasticity with *two director fields* was discussed within the positively defined conventional Frank energy. In the recent paper [54] the authors consider how flexoelectricity combined with spontaneous polar order (ferroelectricity) could stabilize conical spiral orientational order. However, under natural Landau theory assumptions the model in [54] yields strongly biaxial and polar features of the N_{TB} phase, apparently not supported by experimental observations. In [55] a Landau phenomenological theory was proposed for the phase transition from the conventional nematic phase to the heliconical phase. The authors of [55] introduce a double-scale elasticity energy by splitting the director fields into two components: A long-scale Frank energy for a component of the director and a short-scale elastic energy for the remaining component.

As mentioned above, in his seminal paper [42] Dozov proposed higher spatial derivatives of the director nematic field to stabilize his elastic model and to bind the energy from below when K_{33} turns negative. However, there is another way to develop higher order field theories, that is, looking for invariants expressed through higher powers of first derivatives. This approach has certainly been applied with success in several field theories, for example the Skyrme model and the three-dimensional Skyrme-Faddeev model [56–59]. It is in this perspective that, very recently, Virga proposed a new fourth-order generalized elastic theory for nematics [41] with six elastic constants: Three coming from the standard Frank energy second-order terms and the other additional three associated with fourth-order terms. There it was shown how, for a certain choice of two model parameters, two families of uniform distortions with opposite chirality, exhausting the heliconical structures of the N_{TB} phase, minimize the proposed higher order elastic free energy.

In the present paper, after reviewing in a slightly different approach the main results obtained by Virga, we find new localized solutions for the generalized elastic free-energy posited in [41]. On the experimental side, evidence of similar new localized configurations, namely skyrmions, has been found in [14,15], where the authors showed that the existence of either a conical or uniform state surrounding isolated skyrmions leads to an attracting or repulsive interskyrmion potential, respectively. These solitonlike structures in a conical or helical background also appear in ferromagnets. Indeed, not only skyrmions but also the so-called heliknotons were recently investigated both in liquid crystals and ferromagnets [60,61].

The rest of the paper is organized as follows. In Secs. II and III we obtain the main results of Virga's work [41], by expressing the generalized elastic free-energy in terms of the quantities ($\boldsymbol{n}$, $\nabla\boldsymbol{n}$, div$\boldsymbol{n}$, curl$\boldsymbol{n}$) and by analyzing Meyer's heliconical configurations of the N_{TB} phase. We show how a uniform heliconical state corresponds to a minimum of the fourth-order energy density functional for suitable choices of the six elastic constants characterizing Virga's model. In Sec. IV, we approach the problem of searching for nonuniform distortions departing from the uniform heliconical state, finding localized solutions similar to those studied in [62] for the Skyrme-Faddeev model. Finally, we draw our conclusions in Sec. V and we suggest possible extensions of the results here presented.

II. MATHEMATICAL FRAMEWORK

Traditionally, nematic liquid crystals are modeled by a general quadratic form in the spatial gradients $\nabla\boldsymbol{n}$ of a unit vector, the nematic director $\boldsymbol{n}$. This quadratic form is usually known

as Frank's elastic energy density and is written as follows [63]:

$$F_{\rm F} = \tfrac{1}{2}K_{11}(\mathrm{div}\boldsymbol{n})^2 + \tfrac{1}{2}K_{22}(\boldsymbol{n}\cdot\mathrm{curl}\boldsymbol{n})^2 + \tfrac{1}{2}K_{33}|\boldsymbol{n}\times\mathrm{curl}\boldsymbol{n}|^2 + K_{24}[\mathrm{tr}(\nabla\boldsymbol{n})^2 - (\mathrm{div}\boldsymbol{n})^2], \quad (1)$$

where K_{11}, K_{22}, K_{33}, and K_{24} are Frank's elastic constants. The term K_{24} is a *null Lagrangian*; it can be integrated over the domain $\mathcal{B}$ occupied by the nematic medium, without producing any contribution to the total free energy provided that $\boldsymbol{n}$ is assigned over the boundary $\partial\mathcal{B}$. As is customary, the general formula is often reduced to the one-constant approximation, which can be obtained by setting $K_{11} = K_{22} = K_{33} = K$ and $K_{24} = \frac{1}{2}K$, thus leading to

$$F_{\rm F} = \tfrac{1}{2}K||\nabla\boldsymbol{n}||^2, \quad (2)$$

where $||\nabla\boldsymbol{n}||^2 = \partial_i n_k \partial_i n_k$. In [47], a new interpretation of (1) was proposed and analyzed in depth. The starting point of this revisited version of Frank's free-energy density formula is the decomposition of $\nabla\boldsymbol{n}$ in a set of specific distortion modes. More precisely, the gradient of $\boldsymbol{n}$ can be decomposed as follows:

$$\nabla\boldsymbol{n} = -\boldsymbol{b}\otimes\boldsymbol{n} + \tfrac{1}{2}T\mathbf{W}(\boldsymbol{n}) + \tfrac{1}{2}S\mathbf{P}(\boldsymbol{n}) + \mathbf{D}, \quad (3)$$

where the scalar $S = \mathrm{div}\boldsymbol{n}$ is the *splay*, the pseudoscalar $T = \boldsymbol{n}\cdot\mathrm{curl}\boldsymbol{n}$ is the *twist*, and the vector $\boldsymbol{b} = \boldsymbol{n}\times\mathrm{curl}\boldsymbol{n}$ is the *bend*. $\mathbf{W}(\boldsymbol{n})$ denotes the skew-symmetric tensor associated with $\boldsymbol{n}$, i.e., $\mathbf{W}_{ij} = \epsilon_{ijk}n_k$, and $\mathbf{P}(\boldsymbol{n}) = \mathbf{I} - \boldsymbol{n}\otimes\boldsymbol{n}$ is the projector onto the plane orthogonal to $\boldsymbol{n}$. $\mathbf{D}$ is a symmetric traceless tensor such that $\mathbf{D}\boldsymbol{n} = \mathbf{0}$. Accordingly, it can be given the form

$$\mathbf{D} = q(\boldsymbol{n}_1\otimes\boldsymbol{n}_1 - \boldsymbol{n}_2\otimes\boldsymbol{n}_2), \quad (4)$$

where q is the positive eigenvalue of $\mathbf{D}$ and $\boldsymbol{n}_1$ and $\boldsymbol{n}_2$ are the eigenvectors, orthogonal to $\boldsymbol{n}$. From (3) it follows that

$$\mathrm{tr}\mathbf{D}^2 = 2q^2 = \mathrm{tr}(\nabla\boldsymbol{n})^2 + \tfrac{1}{2}T^2 - \tfrac{1}{2}S^2. \quad (5)$$

In coordinates, we can rewrite the director gradient $\nabla\boldsymbol{n}$ as follows [47]:

$$\partial_j n_i = -b_i n_j + \tfrac{1}{2}T\epsilon_{ijk}n_k + \tfrac{1}{2}S(\delta_{ij} - n_i n_j) + D_{ij}, \quad (6)$$

and $\mathbf{D}$ can be given the alternative forms

$$D_{ij} = \tfrac{1}{2}[\partial_i n_j + \partial_j n_i - n_i n_k\partial_k n_j - n_j n_k\partial_k n_i - \delta_{ij}\mathrm{div}\boldsymbol{n} + n_i n_j\mathrm{div}\boldsymbol{n}], \quad (7)$$

or

$$D_{ij} = \tfrac{1}{2}[\partial_i n_j + \partial_j n_i + n_i b_j + n_j b_i - S(\delta_{ij} - n_i n_j)]. \quad (8)$$

The quantity q was named by Selinger [47] as *biaxial splay*. The quantities $(S, T, \boldsymbol{b}, \mathbf{D})$ are independent of one another and are called *measures of distortion*. Frank's elastic free-energy density can be written as a quadratic form in the four above quantities as follows:

$$F_{\rm F} = \tfrac{1}{2}(K_{11} - K_{24})S^2 + \tfrac{1}{2}(K_{22} - K_{24})T^2 + \tfrac{1}{2}K_{33}B^2 + K_{24}\mathrm{tr}(\mathbf{D}^2), \quad (9)$$

where $B^2 = \boldsymbol{b}\cdot\boldsymbol{b}$. As recalled in [41], the positive definiteness of the quadratic form (9) implies that

$$K_{11} - K_{24} > 0, \quad K_{22} - K_{24} > 0, \quad K_{33} > 0, \quad K_{24} > 0, \quad (10)$$

known as Ericksen's inequalities [64]. Accordingly, (9) admits as global minimizer the state

$$S = T = B = q = 0, \quad (11)$$

which corresponds to any constant field $\boldsymbol{n} \equiv \boldsymbol{n_0}$.

As pointed out by the authors in [47], there may be a further surface term in (1), which, in contrast with the saddle-splay term, i.e., the K_{24} term, contains second derivatives of the director. This term reads as $\mathrm{div}(\boldsymbol{n}\,\mathrm{div}\boldsymbol{n}) = S^2 + (\boldsymbol{n}\cdot\nabla)S$. In analogy with what is done for the K_{24} contribution, one can in principle expand $\partial_i\partial_j n_k$ in its normal modes and build a generalized energy density functional with also the second-order part expressed in terms of this modes. However, as recalled by [41] one may obtain a generalized elastic free energy density by introducing higher powers in the expansion of the gradient of $\boldsymbol{n}$. As we will show, these higher order terms, together with the negative sign of K_{33}, are sufficient to accommodate the twist-bend phase as ground state, and no second-derivative term, such as K_{13}, is actually needed.

The eigenvectors $\boldsymbol{n}_1, \boldsymbol{n}_2, \boldsymbol{n}$ of $\mathbf{D}$ are called the *distortion frame*. This can be defined for any sufficiently regular director field $\boldsymbol{n}$ and it changes from point to point, thus defining a movable frame. The bend vector $\boldsymbol{b}$ can be decomposed in the distortion frame as follows:

$$\boldsymbol{b} = b_1\boldsymbol{n}_1 + b_2\boldsymbol{n}_2. \quad (12)$$

The scalars (S, T, b_1, b_2, q) depend on position in space and they are called collectively *distortion characteristics* of the nematic director. In [41] there was introduced the concept of *uniform distortion*, i.e., a uniform distortion is a configuration of the director field $\boldsymbol{n}$ in which the distortion characteristics are the same everywhere, while the distortion frame may change from place to place. Any constant field $\boldsymbol{n} \equiv \boldsymbol{n}_0$ is uniform but with no distortion, thus it is clear that a uniform distortion should also have a nontrivial director pattern. In [41], it was shown that there exist only two families of uniformly distorted director fields, and they are given by

$$S = 0, \quad T = 2q, \quad b_1 = b_2 = b, \quad (13)$$

$$S = 0, \quad T = -2q, \quad b_1 = -b_2 = b, \quad (14)$$

where, of course, q and b are constant assigned parameters. In order to reconstruct the structure of the director fields $\boldsymbol{n}$ corresponding to (13) and (14), one has to integrate the decomposed spatial gradient (3) with the specific distortion characteristics given by (13) and (14). In [41], it was shown that the most general uniform distortion is an *heliconical* director field, more precisely a director field of the form

$$\boldsymbol{n}_h = \sin\theta_0\cos\beta z\boldsymbol{e}_x + \sin\theta_0\sin\beta z\boldsymbol{e}_y + \cos\theta_0\boldsymbol{e}_z, \quad (15)$$

where $\boldsymbol{e}_x, \boldsymbol{e}_y, \boldsymbol{e}_z$ are the Cartesian unit basis vectors in $\mathbb{R}^3$, and the *conical* angle θ_0 and the pitch $2\pi/|\beta|$ are related to the parameters (q, b) as follows:

$$\frac{2\pi}{|\beta|} = \frac{2\pi q}{b^2 + 2q^2}, \quad \cos\theta_0 = \frac{|b|}{\sqrt{b^2 + 2q^2}}. \quad (16)$$

The nematic director $\boldsymbol{n}$ rotates around $\boldsymbol{e}_z$, making a fixed cone angle θ_0 with the rotation axis $\boldsymbol{e}_z$, which is called the helix axis. The distortion frame $\{\boldsymbol{n}_1, \boldsymbol{n}_2, \boldsymbol{n}\}$ precesses along $\boldsymbol{e}_z$ turning completely round over the length of a pitch $2\pi/|\beta|$, and

it remains unchanged in all directions orthogonal to $\boldsymbol{e}_z$. The structure (15) describes therefore the heliconical distortion predicted by Meyer [46] and it corresponds to the *twist-bend* liquid crystal phase, experimentally detected in 2011 [65]. It is worth noticing that formula (15) also describes the nematic phase N when $\theta_0 = 0$ and the chiral nematics when $\theta_0 = \frac{\pi}{2}$, implying that the twist-bend phase represents a structural link between these two extreme phases.

Of course, as also observed in [41] the heliconical configurations cannot be minimizers of the standard Frank elastic energy, and there is need for a new elastic theory able to accommodate the heliconical phase as a ground state. In [41], there was put forward a new energy functional with quartic powers of the spatial gradient of $\boldsymbol{n}$. The starting point for positing the quartic energy functional is the set of measures of distortion $(S, T, \boldsymbol{b}, \mathbf{D})$. In order to form a quartic polynomial in the spatial gradients of $\boldsymbol{n}$ we need to collect the basic invariants under nematic symmetry $\boldsymbol{n} \leftrightarrow -\boldsymbol{n}$, rotations and inversions, i.e.,

$$\{S^2, T^2, B^2, \mathrm{tr}\mathbf{D}^2, S\boldsymbol{b}\cdot\mathbf{D}\boldsymbol{b}, T\boldsymbol{b}\cdot\mathbf{D}(\boldsymbol{n}\times\boldsymbol{b})\}. \tag{17}$$

From the list above it would be possible to construct a general higher order polynomial. However, we shall follow the approach in [41] and we will consider the minimalistic quartic free-energy density as follows:

$$\begin{aligned} F_{TB}(S,T,b_1,b_2,q) = {} & \tfrac{1}{2}k_1S^2 + \tfrac{1}{2}k_2T^2 + k_2\mathrm{tr}\mathbf{D}^2 + \tfrac{1}{2}k_3B^2 \\ & + \tfrac{1}{4}k_4T^4 + k_4(\mathrm{tr}\mathbf{D}^2)^2 + \tfrac{1}{4}k_5B^4 \\ & + k_6T\boldsymbol{b}\cdot\mathbf{D}(\boldsymbol{n}\times\boldsymbol{b}). \end{aligned} \tag{18}$$

This represents the lowest order free-energy density that, for a suitable choice of the elastic constants, admits as global minimizer the heliconical uniform distortion state (15), characterized by (13) and (14), as opposed to the uniform state (11). Notice that other quartic contributions are not included as this is the simplest way to guarantee that the global minimum is attained at (13) and (14).

By taking into account that $\mathrm{tr}\mathbf{D}^2 = 2q^2$ and

$$\boldsymbol{b}\cdot\mathbf{D}(\boldsymbol{n}\times\boldsymbol{b}) = -2qb_1b_2, \tag{19}$$

formula (18) can also be written as a function of the characteristics of distortion,

$$\begin{aligned} F_{TB}(S,T,b_1,b_2,q) = {} & \tfrac{1}{2}k_1S^2 + \tfrac{1}{2}k_2[T^2 + (2q)^2] + \tfrac{1}{2}k_3B^2 \\ & + \tfrac{1}{4}k_4[T^4 + (2q)^4] + \tfrac{1}{4}k_5B^4 \\ & - k_6(2q)Tb_1b_2. \end{aligned} \tag{20}$$

By directly comparing (18) with (9) we get the following formal identification:

$$k_1 = K_{11} - K_{24}, \quad k_2 = K_{22} - K_{24} = K_{24}, \quad k_3 = K_{33}, \tag{21}$$

but as shown below k_3 can also assume negative values. The above energy density turns out to be coercive provided that

$$k_4 > 0, \quad k_5 > 0, \quad k_6 > 0, \quad k_6^2 < 2k_4k_5, \tag{22}$$

which is the condition of positive definiteness of the quartic part of (18). Moreover, since the heliconical states (13) and (14) are characterized by $S = 0$ we assume $k_1 > 0$ so that F_{TB} attains its minimum for $S = 0$. Having fixed conditions on the elastic constants k_1, k_4, k_5, k_6, it makes sense to classify the minimizers in terms of the remaining k_2 and k_3 constants. It was shown in [41] that (18) is minimized by the trivial uniform state $\boldsymbol{n} = \boldsymbol{n}_0$ if and only if $k_3 \geqslant 0$. In terms of the measures of distortions this minimizer is given by (11).

When

$$-2\frac{k_5}{k_6}k_2 < k_3 < 0, \tag{23}$$

the minimizer is a pure bend state with

$$S = T = q = 0, \quad B^2 = b_1^2 + b_2^2 = -\frac{k_3}{k_5}. \tag{24}$$

Finally, when

$$k_3 < -2\frac{k_5}{k_6}k_2 < 0, \tag{25}$$

F_{TB} is minimized by the pure heliconical state

$$\begin{aligned} T^2 = (2q)^2 = -\frac{k_3k_6 + 2k_5k_2}{2k_4k_5 - k_6^2} \geqslant 0 \quad \text{and} \\ b_1^2 = b_2^2 = -\frac{k_2k_6 + k_3k_4}{2k_4k_5 - k_6^2} \geqslant 0. \end{aligned} \tag{26}$$

Summing up, in order to have the heliconical states (26), the following constraints on the elastic constants must hold:

$$2k_4k_5 - k_6^2 > 0, \quad k_3k_6 + 2k_5k_2 < 0, \quad k_2k_6 + k_3k_4 < 0. \tag{27}$$

In the next section we will work out this minimizer by studying the Euler-Lagrange equations associated with F_{TB}. To this end, it is convenient to write F_{TB} in terms of the spatial gradient components $\nabla\boldsymbol{n}$ and of the quantities $\mathrm{div}\boldsymbol{n}$, $\mathrm{curl}\boldsymbol{n}$. For this we need some identities. It can be proved that

$$\begin{aligned} 2Tqb_1b_2 = {} & (\boldsymbol{n}\cdot\mathrm{curl}\boldsymbol{n})\mathrm{curl}\boldsymbol{n}\cdot\nabla\boldsymbol{n}(\boldsymbol{n}\times\mathrm{curl}\boldsymbol{n}) \\ & + \tfrac{1}{2}(\boldsymbol{n}\cdot\mathrm{curl}\boldsymbol{n})^2|\boldsymbol{n}\times\mathrm{curl}\boldsymbol{n}|^2. \end{aligned} \tag{28}$$

Upon this latter identity along with the definitions of S, T, and $\mathbf{D}$ and the identity (5), one arrives at

$$\begin{aligned} F_{TB} = {} & \tfrac{1}{2}(k_1 - k_2)(\mathrm{div}\boldsymbol{n})^2 + k_2(\boldsymbol{n}\cdot\mathrm{curl}\boldsymbol{n})^2 + k_2\mathrm{tr}(\nabla\boldsymbol{n})^2 + \tfrac{1}{2}k_3|\boldsymbol{n}\times\mathrm{curl}\boldsymbol{n}|^2 + \tfrac{1}{4}k_4(\boldsymbol{n}\cdot\mathrm{curl}\boldsymbol{n})^4 \\ & + k_4\big[\mathrm{tr}(\nabla\boldsymbol{n})^2 + \tfrac{1}{2}(\boldsymbol{n}\cdot\mathrm{curl}\boldsymbol{n})^2 - \tfrac{1}{2}(\mathrm{div}\boldsymbol{n})^2\big]^2 + \tfrac{1}{4}k_5|\boldsymbol{n}\times\mathrm{curl}\boldsymbol{n}|^4 \\ & - k_6\big[(\boldsymbol{n}\cdot\mathrm{curl}\boldsymbol{n})\mathrm{curl}\boldsymbol{n}\cdot(\nabla\boldsymbol{n})(\boldsymbol{n}\times\mathrm{curl}\boldsymbol{n}) + \tfrac{1}{2}(\boldsymbol{n}\cdot\mathrm{curl}\boldsymbol{n})^2|\boldsymbol{n}\times\mathrm{curl}\boldsymbol{n}|^2\big]. \end{aligned} \tag{29}$$

Otherwise, F_{TB} can be rewritten as follows:

$$F_{TB} = \tfrac{1}{2}(k_1 - k_2)S^2 + k_2T^2 + k_2\mathrm{tr}(\nabla \boldsymbol{n})^2 + \tfrac{1}{2}k_3B^2 + \tfrac{1}{4}k_4T^4 + k_4\left[\mathrm{tr}(\nabla \boldsymbol{n})^2 + \tfrac{1}{2}T^2 - \tfrac{1}{2}S^2\right]^2 + \tfrac{1}{4}k_5B^4 - k_6I_{4a} - \tfrac{1}{2}k_6T^2B^2, \quad (30)$$

where

$$I_{4a} = [(\boldsymbol{n}\cdot \mathrm{curl}\boldsymbol{n})\mathrm{curl}\boldsymbol{n}\cdot(\nabla \boldsymbol{n})(\boldsymbol{n}\times \mathrm{curl}\boldsymbol{n})]. \quad (31)$$

Correspondingly, the stored free energy in a region $\mathcal{B}$ is given by the volume integral

$$\mathcal{F} = \int_{\mathcal{B}} F_{TB}d\mathcal{B}. \quad (32)$$

III. UNIFORM HELICONICAL DISTORTIONS

In this section we analyze the special class of solutions (13)–(14) which, as shown above, provides a global minimum to the free-energy density functional (29). To this end, we use the standard parametrization of $\boldsymbol{n}$,

$$\boldsymbol{n} = \sin\theta\cos\phi\boldsymbol{e}_x + \sin\theta\sin\phi\boldsymbol{e}_y + \cos\theta\boldsymbol{e}_z, \quad (33)$$

where θ and ϕ are the standard polar angle functions.

The general Euler-Lagrange equations, also supplemented with boundary conditions on $\partial\mathcal{B}$, are rather involved. However, it can be shown that they admit the heliconical configurations (15) as solutions (see [66]). The three-dimensional representation of such configurations is displayed in Fig. 1, where we depict a set of (x, y)-plane cross sections, showing how the configuration changes along z, and a specific helix line. The corresponding free-energy density reads

$$F_{TB}(\boldsymbol{n}_h) = f_{TB}(\theta_0,\beta) = \tfrac{1}{8}\left(-4k_6\cos^2\theta_0\sin^6\theta_0 + 4k_4\sin^8\theta_0 + \tfrac{1}{8}k_5\sin^4 2\theta_0\right)\beta^4 + \tfrac{1}{8}(8k_2\sin^4\theta_0 + k_3\sin^2 2\theta_0)\beta^2, \quad (34)$$

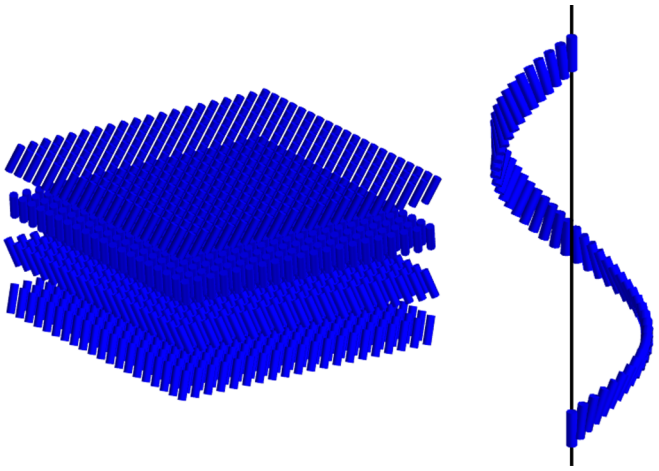

FIG. 1. Three-dimensional representation of the uniform heliconical distortion. *Left:* Different (x, y)-plane cross sections showing the change of orientation along the z direction. *Right*: Helix line along the z axis for a fixed distance from it.

which depends on the pitch-related parameter β and the conical angle θ_0, and is minimized by the values

$$\beta = \pm\frac{(2k_2k_5 + k_3k_6) + 2(k_3k_4 + k_2k_6)}{\sqrt{-(2k_2k_5 + k_3k_6)\left(2k_4k_5 - k_6^2\right)}} \quad (35)$$

and

$$\theta_0 = \arcsin\left(\sqrt{\frac{2k_2k_5 + k_3k_6}{(2k_2k_5 + k_3k_6) + 2(k_3k_4 + k_2k_6)}}\right), \quad (36)$$

with the following condition on the elastic constants:

$$0 < \frac{2k_2k_5 + k_3k_6}{(2k_2k_5 + k_3k_6) + 2(k_3k_4 + k_2k_6)} < 1, \quad (37)$$

fully satisfied by the constraints (27). It is worth noticing that both θ_0 and β do not depend on the elastic constant k_1. Correspondingly, the free-energy density on the heliconical solutions becomes

$$f_{TB}(\theta_0,\beta) = -\frac{1}{2}\frac{k_3^2k_4 + 2k_2^2k_5 + 2k_2k_3k_6}{2k_4k_5 - k_6^2}, \quad (38)$$

which, taking into account (27), turns out to be negative provided that

$$k_3^2k_4 + 2k_2^2k_5 + 2k_2k_3k_6 > 0. \quad (39)$$

Actually, the quadratic form (39) with respect to k_3,

$$k_3^2k_4 + 2k_2^2k_5 + 2k_2k_3k_6, \quad (40)$$

is positive, as the discriminant

$$4k_2^2k_6^2 - 8k_4k_2^2k_5 = 4k_2^2\left(k_6^2 - 2k_4k_5\right) < 0, \quad (41)$$

as a consequence of (27). Thus, the value of the free-energy density at the heliconical state turns out to be lower than the value at the uniform nematic phase.

Finally, it is possible to verify that the heliconical configurations found here correspond to those predicted in [41] in the form (26). Actually, by direct computation, using the expressions for θ_0 and β above, one can show that

$$S = 0, \quad T^2 = \sin^4\theta_0\,\beta^2 = -\frac{2k_2k_5 + k_3k_6}{\left(2k_4k_5 - k_6^2\right)}, \quad \text{and}$$
$$B^2 = b_1^2 + b_2^2 = -\frac{2(k_3k_4 + k_2k_6)}{2k_4k_5 - k_6^2}, \quad (42)$$

which reproduce formulas (26).

IV. NONUNIFORM LOCALIZED STATES

A. Ansatz on the solution

At variance with the previous section, here we consider the case of nonuniform distortions, possibly leading to localized states. Bearing in mind that the uniform distortions are heliconical states, we slightly depart from this case by considering still heliconical structures, but with a nonuniform conical angle and an additional precession around the axis of the uniform heliconical state. More precisely, we consider configurations of the general form

$$\boldsymbol{n}(r, z, \varphi; \alpha, \beta) = \sin[f(r)]\cos(\alpha\varphi + \beta z)\boldsymbol{e}_x + \sin[f(r)] \times \sin(\alpha\varphi + \beta z)\boldsymbol{e}_y + \cos[f(r)]\boldsymbol{e}_z, \quad (43)$$

where α is an integer describing the number of windings performed by the director around the heliconical axis $\boldsymbol{e}_z$ for fixed z, $f(r)$ is the profile function describing the conical angle, and β has the same meaning as in the previous section. In order to have localized configurations, we may impose the boundary conditions $f(0) = 0$ and $f(r \to \infty) = f_0$, f_0 being a suitable conical angle to be determined. Then, to study these configurations, we need to reduce the general free energy in order to translate the ansatz into the equilibrium equations. The reduced free energy integrated over the unit cell $[0, \frac{2\pi}{\beta}] \times [0, 2\pi]$ and over $r \in [0, \infty]$ will take the form

$$\mathcal{F}[f;\alpha,\beta] = \int_0^{\frac{2\pi}{\beta}} dz \int_0^{2\pi} d\varphi \int_0^{\infty} F_{TB}[\boldsymbol{n}(r,z,\varphi;\alpha,\beta)] r\, dr. \tag{44}$$

We are interested in the reduced free-energy per unit cell $[0, \frac{2\pi}{\beta}] \times [0, 2\pi]$ which can be obtained by dividing by the factors 2π and $\frac{2\pi}{\beta}$:

$$\tilde{\mathcal{F}}[f;\alpha,\beta] = \frac{\beta}{4\pi^2}\mathcal{F}[f;\alpha,\beta]. \tag{45}$$

In the following, we will study two relevant cases: $\alpha = 0$ and $\alpha = 1$.

B. Case $\alpha = 0$

In this first case, we are interested in studying whether localized solutions without winding around the heliconical axis $\boldsymbol{e}_z$ are possible. In fact, this is equivalent to taking $\alpha = 0$ in the general ansatz (43) with a radial dependent profile, $f(r)$, for the conical angle. With these assumptions, the reduced free energy reads

$$\mathcal{F}_0[f;\beta] = \int_0^{\infty} [\Gamma_0(f) + \Gamma_2(f) f'^2 + \Gamma_4(f) f'^4] r\, dr, \tag{46}$$

where the quantities Γ_i are functions of the profile $f(r)$, β, and the elastic constants (see the Appendix for details). Hence, the Euler-Lagrange equation is given by

$$2f''(\Gamma_2 + 6f'^2\Gamma_4) + \frac{2}{r}f'\Gamma_2 + f'^2\partial_f\Gamma_2 + \frac{4}{r}f'^3\Gamma_4 + 3f'^4\partial_f\Gamma_4 - \partial_f\Gamma_0 = 0, \tag{47}$$

with $\partial_f\Gamma_i$ the partial derivative of the quantity Γ_i with respect to the conical function f. It is worth noticing that the above equilibrium differential equation is invariant under the following transformation:

$$f \to -f \quad \text{and} \quad r \to -r. \tag{48}$$

First of all, we find the asymptotic state as $r \to \infty$. To this aim, we take the limit of (47) as $r \to \infty$ and we get the asymptotic stationary condition

$$\partial_f\Gamma_0 = 0. \tag{49}$$

This last equation corresponds to a stationary condition for the energy functional (46) in the same limit, $r \to \infty$, where f' also vanishes. Correspondingly, the free-energy per unit cell can be written as

$$\tilde{\mathcal{F}}_0[f;\beta] = \frac{\beta}{4\pi^2}\int \Gamma_0(f) r\, dr + \text{h.o.t.}, \tag{50}$$

where h.o.t. denotes higher order terms. It is clear that in order to find the corresponding asymptotic state we will need to minimize the leading term of (50) with respect to f and β. Thus, in addition to the condition (49) we need to include the stationary condition with respect to β, i.e., letting

$$F_{0\infty}(f,\beta,r) := \frac{\beta}{4\pi^2}\Gamma_0(f) r, \tag{51}$$

we then have to require that

$$\nabla_{(f,\beta)} F_{0\infty}(f,\beta,r) = (0,0). \tag{52}$$

Letting $\tau := \cos 2f$, (51) can be written as

$$F_{0\infty}(\tau,\beta,r) = r\tfrac{1}{64}\beta^2(\tau-1)(\beta^2(\tau-1)[2k_4(\tau-1)^2 + (\tau+1)(k_5 t + k_5 + 2k_6\tau - 2k_6)] + 16k_2(\tau-1) - 8k_3(\tau+1)). \tag{53}$$

The corresponding stationary conditions with respect to β and τ are

$$\tfrac{1}{16}\beta^2(\beta^2(\tau-1)[2k_4(\tau-1)^2 + k_5\tau(\tau+1) + k_6(2\tau+1)(\tau-1)] + 8k_2(\tau-1) - 4k_3\tau) = 0, \tag{54}$$

$$\tfrac{1}{32}\beta(\tau-1)(2\beta^2(\tau-1)[2k_4(\tau-1)^2 + (\tau+1)(k_5\tau + k_5 + 2k_6\tau - 2k_6)] + 16k_2(\tau-1) - 8k_3(\tau+1)) = 0. \tag{55}$$

Upon solving them simultaneously we get solutions τ_0, β as follows:

$$\tau_0 = \frac{-2k_2k_5 + 2k_2k_6 + 2k_3k_4 - k_3k_6}{2k_2(k_5+k_6) + k_3(2k_4+k_6)}, \tag{56}$$

$$\beta = \pm\frac{(2k_2k_5 + k_3k_6) + 2(k_3k_4 + k_2k_6)}{\sqrt{-(2k_2k_5 + k_3k_6)\left(2k_4k_5 - k_6^2\right)}}. \tag{57}$$

The asymptotic conical angle is then given by

$$f_0 = \frac{1}{2}\arccos\tau_0 = \frac{1}{2}\arccos\left(\frac{-2k_2k_5 + 2k_2k_6 + 2k_3k_4 - k_3k_6}{2k_2(k_5+k_6) + k_3(2k_4+k_6)}\right), \tag{58}$$

and is equal to that found in the uniform heliconical state θ_0 (36).

To find localized solutions, we need to solve the Euler-Lagrange equation (47) with some specific boundary conditions. In particular, we require the profile function to reach the asymptotic value of the conical angle θ_0 at infinity, i.e., $f(r) \to \theta_0$ when $r \to \infty$, while at the origin it takes a different value which we will choose as zero for simplicity.

Unfortunately, after checking numerically, we did not find any localized local minima. Thus, the $\alpha = 0$ case just reproduces the uniform heliconical state (15) with a constant conical angle θ_0 as global minimizer. Nevertheless, it seems reasonable to think that the absence of a winding around a given axis makes it difficult to stabilize solutions interpolating different values of the conical angle. Indeed, additional energy is not needed in varying the value of $f(r)$ at the origin and taking the conical angle θ_0 everywhere, arriving at the state corresponding to the global minimum. However, if the system needs to go through an unwinding before reaching the uniform heliconical distortion, then stable local minima may be allowed. This is in fact what happens when $\alpha = 1$, so we will devote the rest of the paper to its study and description.

C. Case $\alpha = 1$

When $\alpha = 1$ the reduced free energy takes the following form

$$\mathcal{F}_1[f;\beta] = \frac{\pi^2}{64\beta}\int_0^\infty [G_0(r,f) + G_1(r,f)f' + G_2(r,f)f'^2 + G_3(r,f)f'^3 + G_4(r,f)f'^4]dr, \tag{59}$$

and the associated Euler-Lagrange equation turns into an ordinary differential equation of second order of the form

$$2f''(G_2 + 3f'G_3 + 6f'^2G_4) + 2f'\partial_r G_2 + f'^2\partial_f G_2 + 2f'^3(\partial_f G_3 + 2\partial_r G_4) + 3f'^4\partial_f G_4 - \partial_f G_0 + \partial_r G_1 = 0. \tag{60}$$

The quantities G_i, $i = 0, 1, 2, 3, 4$ depend on $r, f, \beta, k_1, k_2, k_3, k_4, k_5, k_6$ and are listed below in the Appendix. Also in this case, it is worth noticing that the above equilibrium differential equation is invariant under the transformation

$$f \to -f \quad \text{and} \quad r \to -r. \tag{61}$$

We will use this symmetry property in the following subsections, starting with the investigation of the asymptotic behavior of the profile function $f(r)$ around $r = 0$ and around $r = \infty$.

1. Asymptotics

In order to study the behavior around $r = 0$ we first fix the leading order power at the origin by assuming that, close to $r = 0$, the profile function f takes the form

$$f(r) = ar^l + O(r^{l+1}), \tag{62}$$

with $l > 0$, as a negative value would imply loss of regularity in f at the origin. In addition, l has to take an odd value due to the symmetry given by Eq. (61). Thus, by expanding the left-hand side term of (60) around $f = 0$ which is the value taken by f at $r = 0$, it can be shown (see [66]) that $l = 1$.

Having fixed this leading power, we can now study some relationships among the derivatives of f at $r = 0$ by inspecting the corresponding expansion at $r = 0$. From the above mentioned symmetry property (61) of (60) and from the results about the leading order at $r = 0$, we conclude that the power expansion of f around $r = 0$ takes the form

$$f(r) = \xi r + \zeta r^3 + \eta r^5 + \cdots, \tag{63}$$

where

$$\xi = f'(0), \quad \zeta = \frac{1}{3!}f'''(0), \quad \eta = \frac{1}{5!}f^{(\mathrm{V})}(0), \ldots. \tag{64}$$

By replacing $f(r)$ with (63) in the Euler-Lagrange equation (60), we get an expansion in the even powers of r only. In particular, after a lengthy calculation, we arrive at

$$\zeta = \frac{3\beta^2 k_3\xi + 2(k_1 - 3k_2 - 3\beta^2 k_6)\xi^3}{12(k_1 + 3k_2 + 9k_4\xi^2)}, \tag{65}$$

$$\eta = \frac{1}{360(k_1 + 3k_2 + 9k_4\xi^2)}(30\beta^4 k_5\xi^3 + 120\beta^2 k_2\xi^3 - 80\beta^2 k_3\xi^3 + 30\beta^2 k_3\zeta + 90\beta^2 k_5\xi^5 + 270\beta^2 k_6\xi^5 - 360\beta^2 k_6\xi^2\zeta - 13k_1\xi^5 + 240k_1\xi^2\zeta + 51k_2\xi^5 - 15k_3\xi^5 - 180k_3\xi^2\zeta + 48k_4\xi^7 + 1080k_4\xi^4\zeta - 4320k_4\xi\zeta^2 - 30k_5\xi^7 + 45k_6\xi^7 + 360k_6\xi^4\zeta). \tag{66}$$

This result has been successfully used as a check of the numerical calculations presented below by taking the value of ξ coming from the simulations.

Next we collect the results about the asymptotic analysis as $r \to \infty$ of Eq. (60). From the functions G_i reported in the Appendix, it is not difficult to recognize that the only surviving term is

$$\partial_f G_0^\infty = 0, \tag{67}$$

where the function G_0^∞ is obtained from the function G_0 by dropping all the terms $1/r$ and $1/r^3$ and keeping only linear terms in r, i.e.,

$$G_0^\infty = g_{01}^\infty + g_{02}^\infty \cos 2f + g_{03}^\infty \cos 4f + g_{04}^\infty \cos 6f + g_{05}^\infty \cos 8f, \tag{68}$$

where

$$g_{01}^\infty = \frac{\beta^2}{2}r(192k_2 + 32k_3 + 70\beta^2 k_4 + 3\beta^2 k_5 - 10\beta^2 k_6), \tag{69}$$

$$g_{02}^\infty = -4\beta^2 r(32k_2 + 14\beta^2 k_4 - k_6\beta^2), \tag{70}$$

$$g_{03}^\infty = +2\beta^2 r(16k_2 - 8k_3 + 14\beta^2 k_4 - \beta^2 k_5 + 2\beta^2 k_6), \tag{71}$$

$$g_{04}^{\infty} = -4\beta^4 r(2k_4 + k_6), \tag{72}$$

$$g_{05}^{\infty} = \frac{\beta^4}{2}(2k_4 + k_5 + 2k_6)r, \tag{73}$$

entailing that

$$g_{01}^{\infty} + g_{02}^{\infty} + g_{03}^{\infty} + g_{04}^{\infty} + g_{05}^{\infty} = 0. \tag{74}$$

Correspondingly, from (59), the free-energy per unit cell in the same limit reduces to

$$\tilde{\mathcal{F}}_1[f;\beta] = \frac{1}{256}\int [G_0^{\infty}(r,f)]dr + \text{h.o.t.} \tag{75}$$

Taking into account the expressions for Γ_0 in the Appendix and G_0^{∞}, it should be noticed that the expression for $\tilde{\mathcal{F}}_1[f;\beta]$ is the same as the one obtained for $\tilde{\mathcal{F}}_0[f;\beta]$ in (50). Hence we obtain identical stationary conditions and the same asymptotic state, as far as the conical angle f_0 and β are concerned [see Eqs. (57) for β and (58) for f_0]. As also happened for $\alpha = 0$, the expression for f_0 reproduces the result for θ_0 in (36). Moreover, in order to avoid divergences at infinity of the free-energy density, we also need to subtract (see sections above) the free-energy density value for the uniform helicoidal configuration (general global minimum) from the general free-energy expression. This actually corresponds to the case $\alpha = 0$.

Finally, it is worth noting that the profile $f(r)$ approaches the asymptotical conical angle by means of a modified Bessel function of the second kind and order zero, namely,

$$f(r) = f_0 + \epsilon h(r),$$

$$h(r) = c_2 K_0(\omega r) \approx c_2\sqrt{\frac{\pi}{2}}\frac{e^{-\omega r}}{\sqrt{\omega r}} + \cdots, \tag{76}$$

where c_2 is an arbitrary constant and ω is a parameter coming from the Euler-Lagrange equation and depending on the elastic constants only (see [66]).

2. *Global approximation: Padé approach*

In the previous subsection we analyzed the asymptotic behavior of the solution of Eq. (60) near the boundaries 0 and $+\infty$. Now, one may try to look for an analytic expression that approximates the true solution in some specific sense. To this aim, we take inspiration from similar second-order ODEs involving trigonometric nonlinearities, like the simple pendulum equation or the challenging P_{III} Painlevé equation (see for instance [67]). First, one may apply a suitable transformation in terms of inverse trigonometric functions of the dependent variable, leading to a rational expression of the equation in the new dependent variable and its derivatives. Then, one may more easily study and possibly obtain a suitable approximated solution, with the method adopted, for instance, in [68]. Thus, we look for a solution of the form

$$f(r) = \pi - \arccos[s(r)], \tag{77}$$

where $s(r)$ is an unknown function subject to the conditions

$$\lim_{r\to 0^+} s(r) = -1, \qquad \lim_{r\to+\infty} s(r) = -\cos(f_0), \tag{78}$$

f_0 being defined by the asymptotic value (58). Indeed, the adopted transformation (77) maps (60) into an ODE involving only algebraic rational expressions, i.e., combinations of powers of $s(r)$ and its derivatives, up to the second order, with nonconstant coefficients. However, these coefficients can be Laurent expanded in the neighborhood of the boundaries. Accordingly, one may guess that also the function $s(r)$ could be expressed as a ratio of polynomials in r, possibly of infinite degree. Moreover, having already noted above that $f(r)$ must contain only odd powers of r, it follows from the properties of the arccos function that $s(r)$ must be an even function of r. As a consequence, $s(r)$ and its Taylor expansion must depend on r^2 only. Now, it is well known that Padé approximants are a powerful tool to study the convergence of given Taylor series and they are exact on rational functions [69]. To this end, let $S_N = \sum_{j=0}^{N} c_j r^j$ be a truncated series at the order N of our function $s(r)$; its Padé approximant $s^{[L/M]}$ of order (L, M), $L + M = N$, is given by

$$s^{[L/M]} = \frac{\sum_{j=0}^{L} a_j r^j}{\sum_{j=0}^{M} b_j r^j}, \qquad b_0 = 1, \tag{79}$$

such that

$$S_N - s^{[L/M]} = O(r^{N+1}). \tag{80}$$

In our case we have a boundary value problem with two different series expansions at $r = 0$ and $r = \infty$, respectively, which have to be joined simultaneously by the sought $s^{[L/M]}$. This is a well known problem in the multipoint Padé approximation, which could be solved in terms of continuous fractions (see [69], Vol. 2). However, in the present context, one may proceed in a more straightforward way as follows.

First, by power expanding around $r = 0$ the function $f[s(r)]$ and comparing it with formulas (63) and (64), one obtains the corresponding expansion for $s(r)$,

$$s(r) = -1 + \frac{r^2\xi^2}{2} + \frac{1}{24}r^4(24\xi\zeta - \xi^4) + \frac{1}{720}r^6(720\eta\xi + \xi^6 - 120\xi^3\zeta + 360\zeta^2) + O(r^7). \tag{81}$$

On the other hand, we need a similar expansion at infinity, for which we use the simplest asymptotic expansion,

$$s(r) = -\cos(f_0) + O\left(\frac{1}{r^2}\right). \tag{82}$$

Assuming $f_0 \neq \frac{\pi}{2}$, a possible Padé approximant (79) must have equal highest powers in both numerator and denominator. Thus, one may choose $L = M = 4$, and then set

$$s^{[4/4]} = \frac{a_2 r^4 + a_1 r^2 + a_0}{b_2 r^4 + b_1 r^2 + 1}, \tag{83}$$

where the five constants a_i and b_i have to be determined by using the information contained in both asymptotic expansions above. This can be done by formally expanding $s^{[4/4]}$ around $r = 0$ and $r = \infty$ and by matching the corresponding coefficients with those in (81) and (82). We stop at the fourth order in (81) and, accordingly, the coefficient η, being involved at the sixth order, will not be considered in further calculations. This procedure leads to finding three relations providing the

coefficients a_i, namely

$$a_0 = -1, \quad a_1 = \frac{\xi^2}{2} - b_1,$$
$$a_2 = \frac{1}{24}(12b_1\xi^2 - 24b_2 - \xi^4 + 24\xi\zeta). \tag{84}$$

The constant b_1 can be determined by resorting to (82) and using (84) to obtain

$$b_1 = \frac{-24b_2\cos f_0 + 24b_2 + \xi^4 - 24\xi\zeta}{12\xi^2}. \tag{85}$$

Finally, using the above expressions into $s^{[4/4]}$, one is led to the approximation

$$f(r) = \pi - \arccos\left(\frac{-12b_2r^4\xi^2\cos f_0 + r^2(24b_2\cos f_0 - 24b_2 + 5\xi^4 + 24\xi\zeta) - 12\xi^2}{r^2(-24b_2\cos f_0 + 24b_2 + \xi^4 - 24\xi\zeta) + 12b_2r^4\xi^2 + 12\xi^2}\right). \tag{86}$$

Thus, we are restrained to choosing the four parameters ξ, ζ, b_2, f_0. The most obvious choice for f_0 is to use its expression given by (58) in terms of the elastic constants. Second, the quantity ζ can be expressed in terms of ξ and of the elastic constants by (65). Thus, one can consider the family of functions depending only on the couple (ξ, b_2), which can be determined by a best fit (in the sense of the minimum squares method) with the numerical solution of the differential equation (60). A detailed discussion of these methods and their results is contained in the next section.

3. *Numerical analysis*

Due to the nonlinearity and complexity of the system under consideration, also the use of numerical methods seems mandatory. In the following, we want to numerically study localized solutions of the form (43), with $\alpha = 1$. Here, for notational convenience, we will employ a different symbol for the stored free energy $\mathcal{F}_1$ in (59), i.e.,

$$E_{\alpha=1} = \frac{\pi^2}{64\beta}\int [G_0(r,f) + G_1(r,f)f' + G_2(r,f)f'^2 + G_3(r,f)f'^3 + G_4(r,f)f'^4]dr, \tag{87}$$

where the integration over r is being performed on a finite domain [a similar notation, i.e., $E_{\alpha=0}$, is used for the stored free energy $\mathcal{F}_0$ in (46)]. Hence, to find configurations minimizing this energy we use a gradient flow method in one dimension applied to a lattice of 1000 points with an interspace of $\Delta r = 0.02$. In addition, spatial derivatives are approximated by a finite fourth-order accurate difference. The values of the profile function $f(r)$ at the boundaries of the grid are $f(0) = 0$ and $f(r \to \infty) = \theta_0$; see Eq. (36).

The behavior at the origin comes from the fact that, if we want the field $\boldsymbol{n}$ to be well defined, $f(0)$ has to be zero or an integer multiple of π. Indeed, the condition $f(0) = \pi$ has been also considered but it poses a higher energy with respect to the vanishing profile. This might be expected since it implies a bigger deviation from the global minimum given by the uniform distortion $f = \theta_0$. Figure 2 shows the localized solution with $f(0) = 0$ corresponding to the elastic constants $k_1 = k_2 = k_4 = k_5 = k_6 = 1.0$ and $k_3 = -3.0$, which fulfill all the required constraints (27) and give $\theta_0 = 0.4636$, with the parameter $\beta = 5.0$ as prescribed by analytical expressions (35) and (36). This value has been chosen since it is the

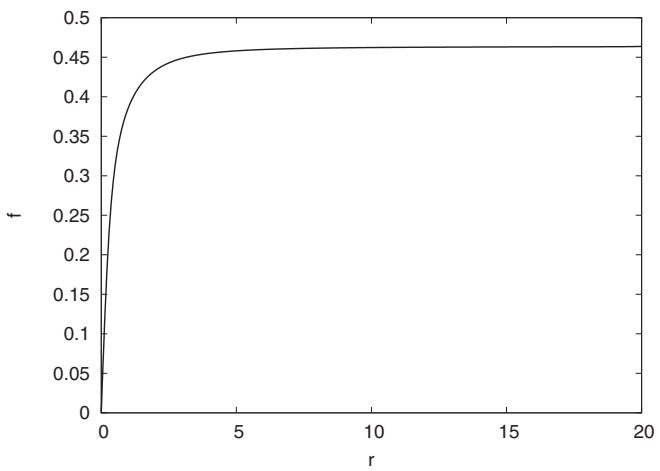

FIG. 2. Profile function $f(r)$ for the elastic constants $k_1 = k_2 = k_4 = k_5 = k_6 = 1.0$ and $k_3 = -3.0$.

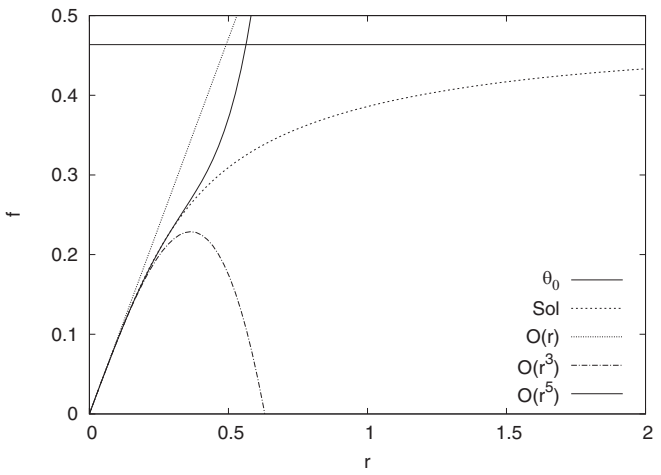

FIG. 3. Profile function $f(r)$ for $k_1 = k_2 = k_4 = k_5 = k_6 = 1.0$ and $k_3 = -3.0$ together with the asymptotic value θ_0 and a representation of the polynomial expansion around $r = 0$ as in (63) to several orders up to r^5 for $\xi = 0.94$.

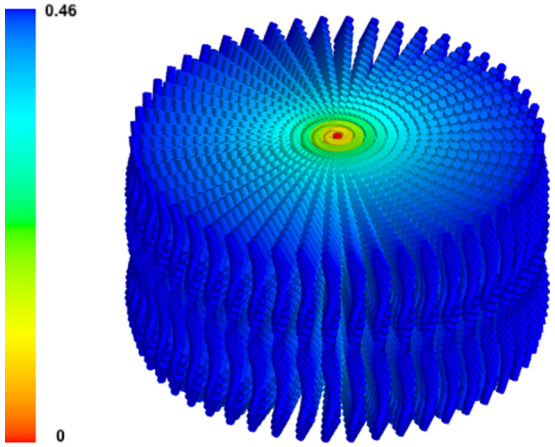

FIG. 4. Three-dimensional reconstruction of the localized solution ($\alpha = 1$) for the elastic constants $k_1 = k_2 = k_4 = k_5 = k_6 = 1.0$ and $k_3 = -3.0$. The color bar represents the value of the conical angle $f(r)$ from the origin to the asymptotic state.

optimal one in the case of the uniform distortion giving the lower energy per pitch $P = \frac{2\pi}{|\beta|}$. In fact, by varying β we have found that, still in the case of localized solutions, $\beta = 5.0$ is the preferred choice, confirming that the analytical expression found for the optimal β is still valid, at least for this choice of the elastic constants. In addition, it seems natural to stick with the analytical expression (35) for β for a better comparison with the case $\alpha = 0$, as this latter reproduces the uniform heliconical state as global minimizer. The energy per pitch of the solution corresponds to $E_{\alpha=1}/P = -3125.97$, while, for the conical distortion (which we can identify with the case $\alpha = 0$ from the general ansatz), $E_{\alpha=0}/P = -3138.45$, which is the relative energy of the excited state $\Delta E/P = (E_{\alpha=1} - E_{\alpha=0})/P = 12.48$. As a check, the behavior of the numerical solution around the origin has been compared with the expansion given by Eq. (63), as shown in Fig. 3. The value of the free parameter of the expansion ξ has been taken from the numerical solution. This result states that the localized nonuniform conical distortions are stable states with respect to the uniform nematic configuration ($\boldsymbol{n} = \boldsymbol{n}_0$), but, at the same time, they can be seen as excitations over the ground

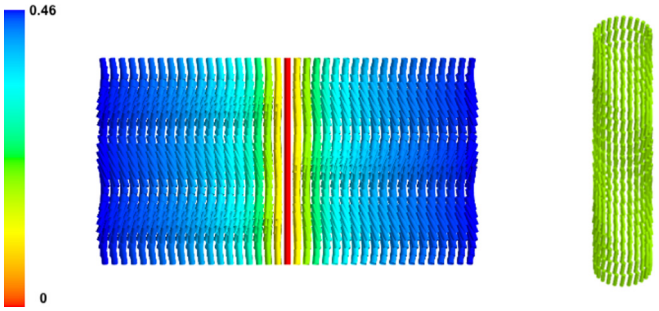

FIG. 5. Transversal cut (left) and cylinder of constant conical angle (right) for the $\alpha = 1$ case. Elastic constant values: $k_1 = k_2 = k_4 = k_5 = k_6 = 1.0$ and $k_3 = -3.0$. The color bar represents the value of the conical angle $f(r)$ from the origin to the asymptotic state.

TABLE I. Energy per pitch and the corresponding excess as a function of k_1 for $k_2 = k_4 = k_5 = k_6 = 1.0$ and $k_3 = -3.0$.

k_1	$E_{\alpha=1}/P$	$\Delta E/P$
1.0	−3125.97	12.48
2.0	−3124.45	14.00
3.0	−3122.99	15.46
4.0	−3121.52	16.93
5.0	−3120.06	18.39
6.0	−3118.61	19.84
7.0	−3117.17	21.28
8.0	−3115.73	22.72
9.0	−3114.31	24.14
10.0	−3112.89	25.56

state realized by the uniform heliconical distortion $\boldsymbol{n} = \boldsymbol{n}_h$; see Eq. (15).

In Fig. 4, we can see the three-dimensional reconstruction of the localized configuration, where the coloring of the bars, representing the vector directors, corresponds to different values of the conical angle given by $f(r)$ as indicated. For a better understanding, this is complemented with the transversal cut on the plane (y, z) appearing in Fig. 5, together with the cylindrical arrangement of those points with the same value of the conical angle.

As previously commented, one can also consider the profile function taking a multiple of π at the origin. However, since this implies a greater deviation from the conical distortion angle, the resulting configuration will have greater energy. For instance, for $f(0) = \pi$, we found that $E_{\alpha=1}/P = -2356.40$, with a relative energy $\Delta E/P = 782.05$.

Another possibility is to study the parameter space, i.e., the elastic constants, of the model. Note that in this case we need to bear in mind the existing constraints (27) involving them. For instance, for a fixed $k_3 = -3.0$, it is not possible to have $k_2 \geqslant 1.5$. Nevertheless, we can see that both β and θ_0 in (35) and (36) do not depend on the elastic constant k_1. Hence, it seems worth studying how the localized configurations

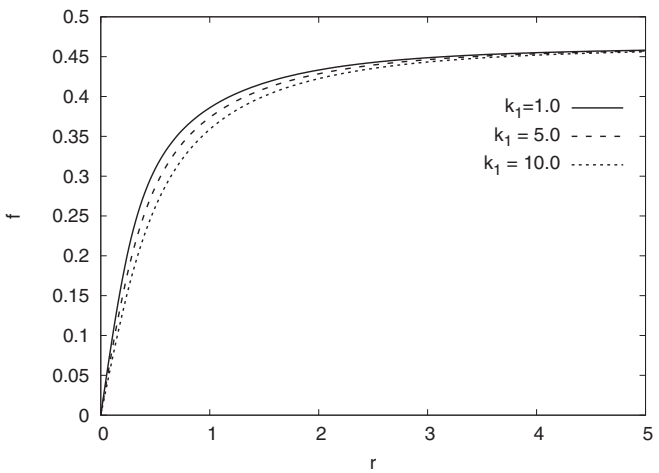

FIG. 6. Profile function $f(r)$ near the origin for an increasing k_1 while $k_2 = k_4 = k_5 = k_6 = 1.0$ and $k_3 = -3.0$. The bigger k_1 is, the slower the asymptotic angle is approached.

TABLE II. Energy per pitch (both of the uniform distortion and localized configuration) and the corresponding excess $\Delta E/P$ as a function of k_4 for $k_1 = k_2 = k_5 = k_6 = 1.0$ and $k_3 = -3.0$.

k_4	β	θ_0	$E_{\alpha=0}/P$	$E_{\alpha=1}/P$	$\Delta E/P$
1.0	5.0	0.4636	−3138.45	−3125.97	12.48
2.0	6.3509	0.3063	−2929.22	−2924.48	4.74
3.0	7.6026	0.2450	−2887.37	−2884.37	3.00
4.0	8.6932	0.2101	−2869.44	−2867.20	2.24
5.0	9.6667	0.1868	−2859.48	−2857.67	1.81
6.0	10.5529	0.1698	−2853.14	−2851.61	1.53
7.0	11.3714	0.1568	−2848.75	−2847.42	1.33
8.0	12.1353	0.1464	−2845.53	−2844.35	1.18
9.0	12.8544	0.1378	−2843.07	−2842.00	1.07
10.0	13.5355	0.1306	−2841.12	-2840.15	0.97

change with an increasing value of it. However, what we find is that as the energy slightly increases (see Table I), so does the size of the configuration (see Fig. 6), although in both cases it does not seem relevant. In particular, regarding the size, it is worth noticing that the bigger k_1 is, the slower the asymptotic angle is approached. On the other hand, there are actually other situations where β and θ_0 change, as can be seen from (35) and (36). For instance, this is the case when one increases the elastic constant k_4. As it can be seen in Table II, this results in a decreasing of the total energy per pitch of both the uniform distortion and the localized configurations. In addition, as can also be seen in Fig. 7, both the excitation energy $\Delta E/P$ and size of the solution are lowered, implying that the latter tends to shrink for an increasing contribution of the elastic constant k_4. Finally, we can also easily study the behavior of the localized solution when decreasing k_3 from -3 to -10 (see Fig. 8 and Table III). In this case, the size also decreases, accompanied by an increasing in the excitation energy. The above numerical results for all the analyzed cases have also been confirmed by using a shooting method for Eq. (60), together with the use of an adaptive mesh in order to cope with the stiffness of the equation around the origin. For

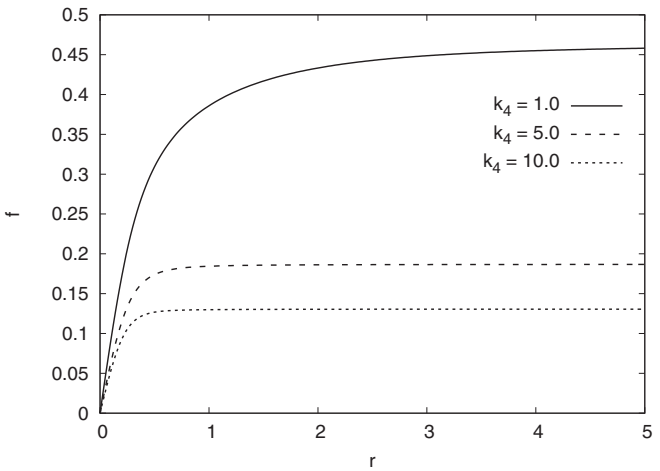

FIG. 7. Profile function $f(r)$ near the origin for an increasing k_4 while $k_1 = k_2 = k_5 = k_6 = 1.0$ and $k_3 = -3.0$. The bigger k_4 is, the faster the asymptotic angle is approached.

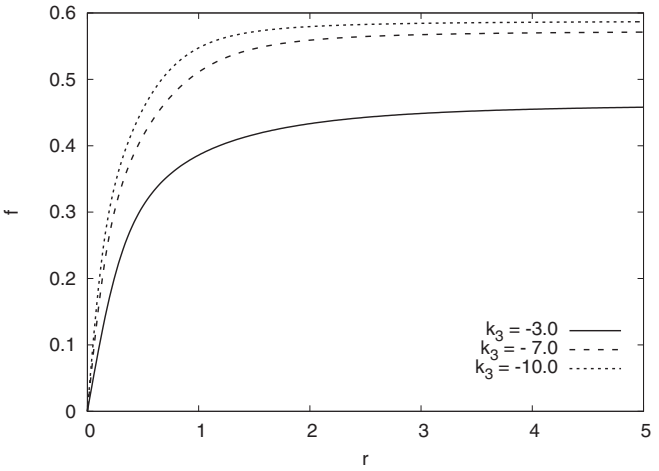

FIG. 8. Profile function $f(r)$ near the origin for a decreasing k_3 while $k_1 = k_2 = k_4 = k_5 = k_6 = 1.0$. The bigger $|k_3|$ is, the faster the asymptotic angle is approached.

this alternative numerical method the normal form of Eq. (60) has been used as reported in [66].

Now that we have studied the solutions to Eq. (60) by numerical methods, we can check the goodness of approximation (86) by a best fitting procedure. As mentioned above, the number of free parameters for least-squares minimization can be reduced to 2, i.e., (ξ, b_2), by means of (58) and (65). However, here first we use all four parameters (ξ, ζ, b_2, f_0) for a few examples. Then we provide the results of the fitting procedure leaving free only (ξ, b_2) or just b_2 (with ξ fixed by numerics), for the case $k_1 = k_2 = k_4 = k_5 = k_6 = 1.0$, $k_3 = -3.0$ shown in Fig. 2. By doing so, we show the remarkable capability of (86) to adapt itself to the numerical solutions.

The results of the procedure using all the four possible parameters are provided in Table IV for four different sets $\{k_i\}$. Here, the values of the best fitting parameters together with the reference values ξ_{num}, ζ_{num} extrapolated from numerical solutions are provided. As an estimator of the goodness of the best fit, we report in the last column the distance $||f - f_a||_2$ between the numerical solution f and the approximation f_a, the latter value being obtained by replacing in (86) the parameters (ξ, ζ, b_2, f_0) with the best fitted ones.

TABLE III. Energy per pitch (both of the uniform distortion and localized configuration) and the corresponding excess as a function of k_3 for $k_1 = k_2 = k_4 = k_5 = k_6 = 1.0$.

k_3	β	θ_0	$E_{\alpha=0}/P$	$E_{\alpha=1}/P$	$\Delta E/P$
−3.0	5.0	0.4636	−3138.45	−3125.97	12.48
−4.0	5.6569	0.5236	−6276.90	−6250.90	26.00
−5.0	6.3509	0.5495	−10670.7	−10629.9	40.8
−6.0	7.0	0.5639	−16319.9	−16263.6	56.3
−7.0	7.6026	0.5732	−23224.5	−23152.0	72.5
−8.0	8.1650	0.5796	−31384.5	−31295.4	89.1
−9.0	8.6932	0.5844	−40799.9	−40693.8	106.1
−10.0	9.1924	0.5880	−51470.6	−51347.2	123.4

TABLE IV. Results of the best fitting procedure for four different sets of $\{k_i\}$: $k_1 = k_2 = k_4 = k_5 = k_6 = 1,\ k_3 = -3$ (Case 1); $k_1 = k_2 = k_5 = k_6 = 1,\ k_3 = -3,\ k_4 = 5$ (Case 2); $k_1 = 10,\ k_2 = k_4 = k_5 = k_6 = 1,\ k_3 = -3$ (Case 3); $k_1 = k_4 = k_5 = k_6 = 1,\ k_2 = 3,\ k_3 = -7$ (Case 4). The quantities ξ_{num} and ζ_{num} represent the values obtained from numerical solutions, while f_a is the approximation obtained by replacing in (86) the parameters (ξ, ζ, b_2, f_0) with the best fitted ones. f_0 is obtained from the best fit and it reproduces up to the fourth decimal digit the value from (58).

Case	ξ	ξ_{num}	ζ	ζ_{num}	f_0	b_2	$\|\|f - f_a\|\|_2$
1	0.9620	0.9465	−2.8997	−2.3733	0.4637	3.9775	0.0063
2	0.6604	0.6650	−2.1686	−2.5290	0.1868	95.2940	0.0015
3	0.6854	0.6793	−1.0512	−0.9496	0.4637	1.9905	0.0077
4	1.4608	1.4400	−13.8035	−11.4797	0.3368	41.6260	0.0024

Moreover, the latter results are depicted in Fig. 9, in order to provide a visual representation of them. Finally, the detailed analysis, with two and one free parameters respectively, for the case $k_1 = k_2 = k_4 = k_5 = k_6 = 1, k_3 = -3$ is displayed in Fig. 10.

According to these results, we can conclude that (86) is a quite good approximation for the solutions of (60).

V. CONCLUSIONS AND PERSPECTIVES

In this paper we studied a generalized elasticity theory for liquid crystals put forward recently in [41], parametrized by six elastic constants: k_1, k_2, k_3 coming from the standard Frank energy second-order contributions and k_4, k_5, k_6 related to the fourth-order terms, as shown in Eq. (18) and constrained by

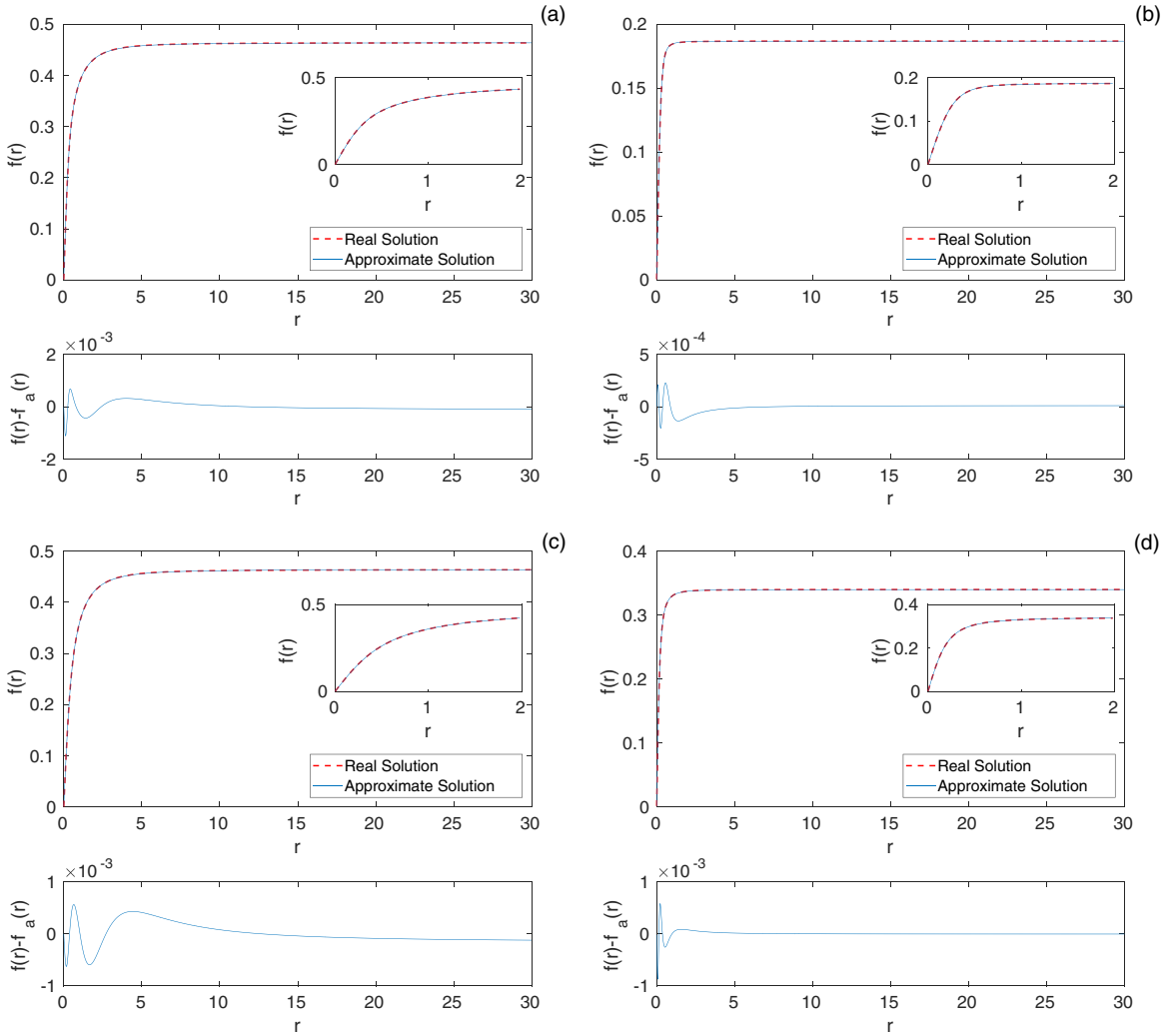

FIG. 9. Best fits between the numerical solution and approximation (86) corresponding to the cases listed in Table IV: (a) $k_1 = k_2 = k_4 = k_5 = k_6 = 1,\ k_3 = -3$; (b) $k_1 = k_2 = k_5 = k_6 = 1,\ k_3 = -3,\ k_4 = 5$; (c) $k_1 = 10,\ k_2 = k_4 = k_5 = k_6 = 1,\ k_3 = -3$; (d) $k_1 = k_4 = k_5 = k_6 = 1,\ k_2 = 3,\ k_3 = -7$.

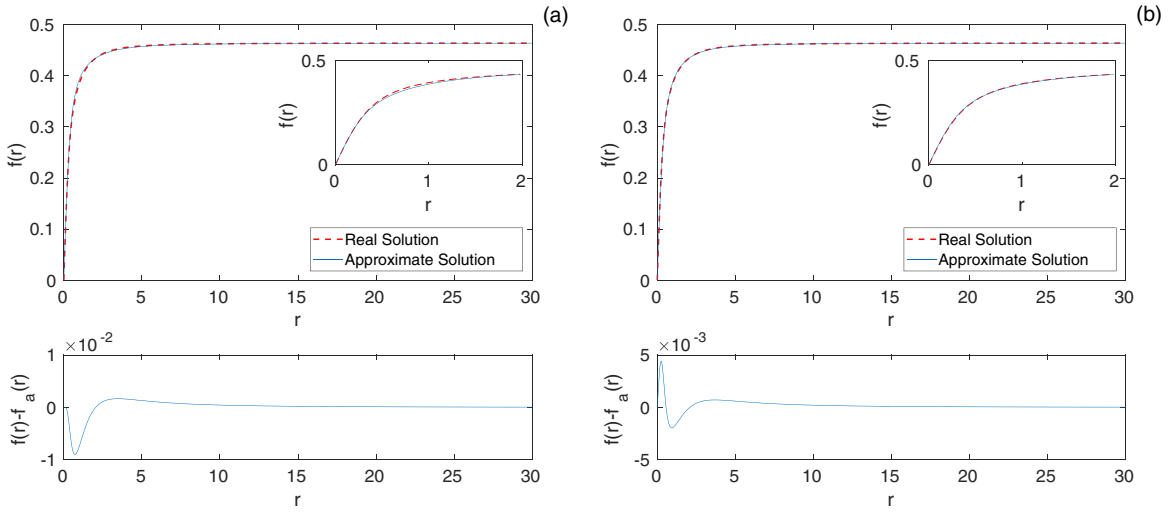

FIG. 10. Best fits between the numerical solution and approximation (86) leaving free (a) b_2 and (b) both ξ, b_2, for the case $k_1 = k_2 = k_4 = k_5 = k_6 = 1, k_3 = -3$. Here (a) $b_2 = 1.4884$ and (b) $(b_2, \xi) = (2.5594, 0.9217)$.

Eq. (27). The quartic part, positive definite, is needed to stabilize the negative contribution from $k_3 < 0$ for the heliconical phase to take place. Thus, the proposed theory generalizes Frank's elastic energy density to include quartic terms in the spatial gradients of the nematic director. For a suitable choice of the elastic constants, the novel free-energy functional admits heliconical configurations as ground state. These ground states have been determined by minimizing the free-energy density with respect to the two parameters, β and θ_0, of the heliconical solution. In the present paper we have adopted a different approach, using the Euler-Lagrange equations. We determined the pitch and the conical angle of the heliconical configurations. After that, we generalized the heliconical configurations to nonuniform structures with a variable conical angle (43). The generalized solution contains two parameters α, β and a profile function for the conical angle depending on the radial distance from the symmetry axis of the configuration. We have studied the Euler-Lagrange equation associated with the reduced functional on this family of solutions in two distinct cases: $\alpha = 0$ and $\alpha = 1$. This α parameter describes only how the vector director winds around the z axis (see Fig. 11). When it vanishes there is no winding, while it goes around the z axis once when $\alpha = 1$. These structures may resemble vortexlike configurations, with α taking the role of the vortex charge. We have performed both numerical and analytical studies and we found a nonuniform profile function only in the case $\alpha = 1$. Case $\alpha = 0$ corresponds to the uniform heliconical solutions found in [41]; its structure is a pile of different strata, each of them with the same constant conical angle θ_0, as shown in Fig. 1, continuously precessing when moving parallel to the z axis. In contrast, when $\alpha = 1$, there is a simultaneous bending of the conical angle, from 0 to θ_0 in the radial direction, which is precessing both in the z direction and by azimuthal rotations. Thus, a helix appears as a line for each fixed constant director, together with the already mentioned winding around the z axis. The corresponding energy still remains under the uniform nematic configuration. However, the system needs to go through an unwinding before reaching the uniform heliconical distortion, and in this sense these solutions can be seen as stable excitations of that ground state.

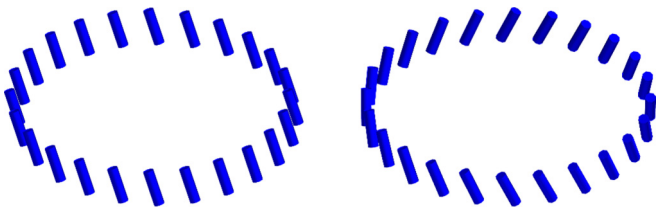

FIG. 11. Circle of constant radius for the solutions of $\alpha = 0$ (left) and $\alpha = 1$ (right) far from the origin at fixed z. Elastic constant values: $k_1 = k_2 = k_4 = k_5 = k_6 = 1.0$ and $k_3 = -3.0$.

It is worth comparing our results with the work presented in [14,15]. There, similar configurations called Skyrmion tubes are numerically described in ferromagnets, while experimentally they are found in liquid crystals. However, although similarities between ferromagnets and liquid crystals are well known, there was no theoretical description for this kind of configuration in achiral nematics in the absence of external fields. Then, to the best of our knowledge, the quartic-degree free-energy proposed by Virga and studied here is the first theory of liquid crystals supporting these localized structures.

Indeed, our solutions described above are quite similar to those in [14,15], with the main difference being the asymptotic behavior far from the origin. In contrast to their case, where the vector director achieves the uniform distortion state (the case $\alpha = 0$ in our language), ours is given by a vector director with a constant conical angle, but presenting a winding around the symmetry axis as well. Hence, the configurations studied here might provide a good description of the cores of the Skyrmion tubes. The similarities between our configurations and those found in cholesterics should not surprise. In chiral ferromagnets and liquid crystals the lack of inversion symmetry, due to the presence of the antisymmetric contributions like the Dzyaloshinskii-Moriya interaction or $q_0 \boldsymbol{n} \cdot \mathrm{curl}\boldsymbol{n}$, together with the frustration from geometric confinement and external fields, creates competing effects which may lead to the formation of a vast class of defects in the

director distribution, either topological or not. Although in our case the inversion symmetry still holds, a similar mechanism of competition between the quadratic part of the functional with negative k_3 and the positive-definite quartic part leads to nontrivial localized configurations like those we found, even in the absence of external frustration. On the other hand, it should be noted that we have shown how, far from the origin, the dominant contribution to the free energy is exactly the same both for $\alpha = 0$ and for $\alpha = 1$ cases, so, at least at that level, they are equivalent. Thus, despite the cylindrical symmetry of our ansatz preventing us from joining the winding localized solution with $\alpha = 1$ to the uniform distortion, this seems to indicate that the skyrmionic structures in [14,15] may also be supported by this quartic theory. Although it is outside the scope of this paper, a more general ansatz will be pursued in the future.

In this paper, we have shown how the first nonzero higher (quartic) order terms in a theory with negative k_3 can host localized distortions in achiral nematics, while the Frank-Oseen quadratic free-energy functional allows them only in the chiral case under external fields. This suggests that structures resembling our solutions might be experimentally found without applying external fields.

On the other hand, the expression given in (86) opens new possibilities in the study of field equations of interest, like (60), in the domain of Skyrmions and similar configurations in liquid crystals and magnetic materials. Generally, they are only addressed by numerical methods, because of the complicated structure of different effects at different scales. In our particular case, these effects are related to the singularities in the coefficients at the origin and the appearance of the trigonometric multiple field contributions in the free energy. The procedure leading to (86) is based on a systematic and algorithmic manipulation of analytic expressions which closely reproduce the numerical solutions, even if they do not provide the exact results. In order to obtain this, the method of the Padé approximants has played an important role. Actually, by our mixed method we proved that the fourth-order approximant already provides an accuracy of 10^{-3} in reproducing the numerical solution, by a suitable choice of the parameters.

In the future, we would like to develop and apply a coherent procedure leading to an accurate *a priori* evaluation of the Padé coefficients at a given order of approximation. The study of the singularities of the approximated solution in the complex r plane may indicate how to tackle such a problem in an efficient way, e.g., moving or adding poles on suitable conjugated points.

In addition, we also plan to study the interactions of the obtained localized structures among themselves and the effect of the interaction with external electric and/or magnetic fields in order to control the main structure parameters. We also aim at studying the proposed quartic free-energy functional in confined geometries for liquid crystals.

ACKNOWLEDGMENTS

G.D.M. is supported by the Dipartimento di Matematica e Fisica "E. De Giorgi," University of Salento grant *Studio analitico di configurazioni spazialmente localizzate in materia condensata e materia nucleare*. C.N. is supported by the INFN grant 19292/2017 (MMNLP) *Integrable Models and Their Applications to Classical and Quantum Problems*. L.M. has been partially supported by INFN IS-MMNLP. V.T. is partially supported by the Italian Ministry of Education, University and Research MIUR.

APPENDIX: MATHEMATICAL DETAILS

In this Appendix we collect the basic main functions and coefficients appearing in the equilibrium equations for both cases $\alpha = 0$ and $\alpha = 1$.

1. Case: $\alpha = 0$

The quantities $\Gamma_i(f)$, with $i = 0, 2, 4$, involved in the reduced free-energy for $\alpha = 0$ [see Eqs. (46) and (47) in the main text] are given by

$$\Gamma_0(f) = \gamma_{01} + \gamma_{02}\cos(2f) + \gamma_{03}\cos(4f) + \gamma_{04}\cos(6f) + \gamma_{05}\cos(8f), \tag{A1}$$

with coefficients

$$\gamma_{01} = \frac{\pi^2}{128}\beta[32(6k_2 + k_3) + (70k_4 + 3k_5 - 10k_6)\beta^2], \tag{A2}$$

$$\gamma_{02} = -\frac{\pi^2}{16}\beta[32k_2 + (14k_4 - k_6)\beta^2], \tag{A3}$$

$$\gamma_{03} = \frac{\pi^2}{32}\beta[16k_2 - 8k_3 + (14k_4 - k_5 + 2k_6)\beta^2], \tag{A4}$$

$$\gamma_{04} = -\frac{\pi^2}{16}(2k_4 + k_6)\beta^3, \tag{A5}$$

$$\gamma_{05} = \frac{\pi^2}{128}(2k_4 + k_5 + 2k_6)\beta^3. \tag{A6}$$

Then

$$\Gamma_2(f) = \gamma_{21} + \gamma_{22}\cos 2f + \gamma_{23}\cos 4f + \gamma_{24}\cos 6f, \tag{A7}$$

with

$$\gamma_{21} = \frac{\pi^2}{32\beta}(16k_1 + 80k_2 + 16k_3 + 74\beta^2 k_4 + 2\beta^2 k_5 + 18\beta^2 k_6), \tag{A8}$$

$$\gamma_{22} = \frac{\pi^2}{32\beta}(16k_1 + 16k_2 - 16k_3 - 97\beta^2 k_4 - \beta^2 k_5 - 17\beta^2 k_6), \tag{A9}$$

$$\gamma_{23} = \frac{\pi^2}{32}\beta(22k_4 - 2k_5 - 2k_6), \tag{A10}$$

$$\gamma_{24} = \frac{\pi^2}{32}\beta(k_4 + k_5 + k_6). \tag{A11}$$

And finally,

$$\Gamma_4(f) = \gamma_{41} + \gamma_{42}\cos(2f) + \gamma_{43}\cos(4f), \tag{A12}$$

with

$$\gamma_{41} = \frac{\pi^2}{64\beta}(65k_4 + 9k_5 - 8k_6), \tag{A13}$$

$$\gamma_{42} = \frac{\pi^2}{64\beta}(20k_4 - 12k_5 + 8k_6), \tag{A14}$$

$$\gamma_{43} = \frac{\pi^2}{64\beta}(3k_4 + 3k_5). \tag{A15}$$

2. Case: $\alpha = 1$

The quantities G_i, $i = 0, 1, 2, 3, 4$ appearing in Eq. (60) depend on $r, f, \beta, k_1, k_2, k_3, k_4, k_5, k_6$ and are listed below:

$$G_0 = G_0(r, f) = g_{01} + g_{02}\cos(2f) + g_{03}\cos(4f) + g_{04}\cos(6f) + g_{05}\cos(8f), \tag{A16}$$

where

$$g_{01} = \frac{1}{16r^3}(178k_4 + 105k_5 - 30k_6) + \frac{1}{2r}(64k_1 + 96k_2 + 48k_3 + 70\beta^2k_4 + 15\beta^2k_5 - 18\beta^2k_6) + \frac{\beta^2}{2}r(192k_2 + 32k_3 + 70\beta^2k_4 + 3\beta^2k_5 - 10\beta^2k_6), \tag{A17}$$

$$g_{02} = -\frac{1}{2r^3}(25k_4 + 21k_5 - 3k_6) - \frac{32}{r}(k_1 + k_2 + k_3) - \frac{2\beta^2}{r}(21k_4 + 3k_5 - 10k_6) - 4\beta^2 r(32k_2 + 14\beta^2k_4 - k_6\beta^2), \tag{A18}$$

$$g_{03} = \frac{1}{4r^3}(2k_4 + 21k_5 + 6k_6) - \frac{2}{r}(8k_2 - 4k_3 + 3\beta^2k_5 + 10\beta^2k_6) + 2\beta^2 r(16k_2 - 8k_3 + 14\beta^2k_4 - \beta^2k_5 + 2\beta^2k_6), \tag{A19}$$

$$g_{04} = -\frac{1}{2r^3}(-k_4 + 3k_5 + 3k_6) + \frac{2\beta^2}{r}(5k_4 + 3k_5 + 6k_6) - 4\beta^4 r(2k_4 + k_6), \tag{A20}$$

$$g_{05} = (2k_4 + k_5 + 2k_6)\left(\frac{3}{16r^3} - \frac{3\beta^2}{2r} + \frac{\beta^4}{2}r\right), \tag{A21}$$

with

$$g_{01} + g_{02} + g_{03} + g_{04} + g_{05} = 0. \tag{A22}$$

G_1 is

$$G_1 = G_1(r, f) = g_{11}\sin(2f) + g_{12}\sin(4f) + g_{13}\sin(6f), \tag{A23}$$

where

$$g_{11} = \frac{1}{r^2}(-35k_4 + 5k_6) + 64(k_1 - k_2) - 20(k_4 + k_6)\beta^2, \tag{A24}$$

$$g_{12} = \frac{4}{r^2}(4k_4 - k_6) + 16(k_4 + k_6)\beta^2, \tag{A25}$$

$$g_{13} = \frac{1}{r^2}(k_4 + k_6) - 4(k_4 + k_6)\beta^2. \tag{A26}$$

G_2 is

$$G_2 = G_2(r, f) = g_{21} + g_{22}\cos(2f) + g_{23}\cos(4f) + g_{24}\cos(6f), \tag{A27}$$

where

$$g_{21} = \frac{1}{r}(71k_4 + 5k_5 + 29k_6) + 4r[8(k_1 + 5k_2 + k_3) + \beta^2(37k_4 + k_5 + 9k_6)], \tag{A28}$$

$$g_{22} = -\frac{1}{2r}(15k_4 + 15k_5 + 79k_6) + 2r[16(k_1 + k_2 - k_3) - \beta^2(97k_4 + k_5 + 17k_6)], \tag{A29}$$

$$g_{23} = \frac{1}{r}(-63k_4 + 3k_5 + 11k_6) + 4\beta^2 r(11k_4 - k_5 - k_6), \tag{A30}$$

$$g_{24} = (k_4 + k_5 + k_6)\left(2\beta^2 r - \frac{1}{2r}\right). \tag{A31}$$

The function G_3 is given by

$$G_3 = G_3(f) = g_{31}\sin(2f) + g_{32}\sin(4f), \tag{A32}$$

where

$$g_{31} = -8(6k_4 + k_6), \tag{A33}$$

$$g_{32} = -4(4k_4 - k_6). \tag{A34}$$

Finally,

$$G_4 = G_4(r, f) = g_{41} + g_{42}\cos(2f) + g_{43}\cos(4f), \tag{A35}$$

where

$$g_{41} = r(65k_4 + 9k_5 - 8k_6), \tag{A36}$$

$$g_{42} = 4r(5k_4 - 3k_5 + 2k_6), \tag{A37}$$

$$g_{43} = 3r(k4 + k5). \tag{A38}$$

[1] P. De Gennes and J. Prost, *The Physics of Liquid Crystals* (Clarendon Press, Oxford, 1993).

[2] I. W. Stewart, *The Static and Dynamic Continuum Theory of Liquid Crystals* (Taylor & Francis, London, 2004).

[3] M. J. Stephen and J. P. Straley, Rev. Mod. Phys. **46**, 617 (1974).

[4] D. C. Wright and N. D. Mermin, Rev. Mod. Phys. **61**, 385 (1989).

[5] R. D. Kamien and J. V. Selinger, J. Phys.: Condens. Matter **13**, R1 (2001).

[6] J. Baudry, S. Pirkl, and P. Oswald, Phys. Rev. E **59**, 5562 (1999).

[7] P. Oswald, J. Baudry, and S. Pirkl, Phys. Rep. **337**, 67 (2000).

[8] G. De Matteis, L. Martina, and V. Turco, Theor. Math. Phys. **196**, 1150 (2018).

[9] G. De Matteis, L. Martina, C. Naya, and V. Turco, Phys. Rev. E **100**, 052703 (2019).

[10] S. Afghah and J. V. Selinger, Phys. Rev. E **96**, 012708 (2017).

[11] J. Fukuda and S. Žumer, Nat. Commun. **2**, 246 (2011).

[12] I. I. Smalyukh, Y. Lansac, N. A. Clark, and R. P. Trivedi, Nat. Mater. **9**, 139 (2010).

[13] P. J. Ackerman, R. P. Trivedi, B. Senyuk, J. van de Lagemaat, and I. I. Smalyukh, Phys. Rev. E **90**, 012505 (2014).

[14] H. R. O. Sohn, S. M. Vlasov, V. M. Uzdin, A. O. Leonov, and I. I. Smalyukh, Phys. Rev. B **100**, 104401 (2019).

[15] A. O. Leonov, A. N. Bogdanov, and K. Inoue, Phys. Rev. B **98**, 060411(R) (2018).

[16] D. Chen, J. H. Porada, J. B. Hooper, A. Klittnick, Y. Shen, M. R. Tuchband, E. Korblova, D. Bedrov, D. M. Walba, M. A. Glaser, J. E. Maclennan, and N. A. Clark, Proc. Natl. Acad. Sci. USA **110**, 15931 (2013).

[17] V. Borshch, Y.-K. Kim, J. Xiang, M. Gao, A. Jákli, V. P. Panov, J. K. Vij, C. T. Imrie, M. G. Tamba, G. H. Mehl, and O. D. Lavrentovich, Nat. Commun. **4**, 2635 (2013).

[18] H. Takezoe and A. Eremin, *Bent-Shaped Liquid Crystals: Structures and Physical Properties* (CRC Press, Boca Raton, FL, 2017).

[19] J. Xiang, S. V. Shiyanovskii, C. T. Imrie, and O. D. Lavrentovich, Phys. Rev. Lett. **112**, 217801 (2014).

[20] J. Xiang, Y. Li, Q. Li, D. A. Paterson, J. M. D. Storey, C. T. Imrie, and O. D. Lavrentovich, Adv. Mater. **27**, 3014 (2015).

[21] J. Xiang, A. Varanytsia, F. Minkowski, D. A. Paterson, J. M. D. Storey, C. T. Imrie, O. D. Lavrentovich, and P. Palffy-Muhoray, Proc. Natl. Acad. Sci. USA **113**, 12925 (2016).

[22] S. M. Salili, J. Xiang, H. Wang, Q. Li, D. A. Paterson, J. M. D. Storey, C. T. Imrie, O. D. Lavrentovich, S. N. Sprunt, J. T. Gleeson, and A. Jákli, Phys. Rev. E **94**, 042705 (2016).

[23] O. S. Iadlovska, G. Babakhanova, G. H. Mehl, C. Welch, E. Cruickshank, G. J. Strachan, J. M. D. Storey, C. T. Imrie, S. V. Shiyanovskii, and O. D. Lavrentovich, Phys. Rev. Res. **2**, 013248 (2020).

[24] C. Greco, G. R. Luckhurst, and A. Ferrarini, Soft Matter **10**, 9318 (2014).

[25] Ya. B. Zel'dovich, Zh. Eksp. Teor. Fiz. **67**, 2357 (1974) [Sov. Phys. JETP **40**, 1170 (1975)].

[26] I. E. Dzyaloshinskii, S. G. Dmitriev, and E. I. Kats, Zh. Eksp. Teor. Fiz. **68**, 2335 (1975) [Sov. Phys. JETP **41**, 1167 (1975)].

[27] S. M. Salili, C. Kim, S. Sprunt, J. T. Gleeson, O. Parri, and A. Jákli, RSC Adv. **4**, 57419 (2014).

[28] K. L. Atkinson, S. M. Morris, F. Castles, M. M. Qasim, D. J. Gardiner, and H. J. Coles, Phys. Rev. E **85**, 012701 (2012).

[29] R. Balachandran, V. P. Panov, Y. P. Panarin, J. K. Vij, M. G. Tamba, G. H. Mehl, and J. K. Song, J. Mater. Chem. C **2**, 8179 (2014).

[30] R. R. Ribeiro de Almeida, C. Zhang, O. Parri, S. N. Sprunt, and A. Jákli, Liq. Cryst. **41**, 1661 (2014).

[31] P. A. Henderson and C. T. Imrie, Liq. Cryst. **38**, 1407 (2011).

[32] T. Ivsic, M. Vinkovic, U. Baumeister, A. Mikleusevic, and A. Lesac, Soft Matter **10**, 9334 (2014).

[33] K. Adlem, M. Čopič, G. R. Luckhurst, A. Mertelj, O. Parri, R. M. Richardson, B. D. Snow, B. A. Timimi, R. P. Tuffin, and D. Wilkes, Phys. Rev. E **88**, 022503 (2013).

[34] N. Sebastián, D. O. Lopez, B. Robles-Hernandez, M. R. de la Fuente, J. Salud, M. A. Perez-Jubindo, D. A. Dunmur, G. R. Luckhurst, and D. J. B. Jackson, Phys. Chem. Chem. Phys. **16**, 21391 (2014).

[35] N. Sebastián, M. G. Tamba, R. Stannarius, M. R. de la Fuente, M. Salamonczyk, G. Cukrov, J. Gleeson, S. Sprunt, A. Jákli, C. Welch, Z. Ahmed, G. H. Mehl, and A. Eremin, Phys. Chem. Chem. Phys. **18**, 19299 (2016).

[36] L. Longa and G. Pajak, Phys. Rev. E **93**, 040701(R) (2016).

[37] E. G. Virga, Phys. Rev. E **89**, 052502 (2014).

[38] G. Barbero, L. R. Evangelista, M. P. Rosseto, R. S. Zola, and I. Lelidis, Phys. Rev. E **92**, 030501(R) (2015).

[39] R. S. Zola, G. Barbero, I. Lelidis, M. P. Rosseto, and L. R. Evangelista, Liq. Cryst. **44**, 24 (2017).

[40] R. S. Zola, R. R. Ribeiro de Almelda, G. Barbero, I. Lelidis, D. S. Dalcol, M. P. Rosseto, and L. R. Evangelista, Mol. Cryst. Liq. Cryst. **649**, 71 (2017).

[41] E. G. Virga, Phys. Rev. E **100**, 052701 (2019).

[42] I. Dozov, Europhys. Lett. **56**, 247 (2001).

[43] S. Kaur, J. Addis, C. Greco, A. Ferrarini, V. Gortz, J. W. Goodby, and H. F. Gleeson, Phys. Rev. E **86**, 041703 (2012).

[44] C. Meyer, G. R. Luckhurst, and I. Dozov, Phys. Rev. Lett. **111**, 067801 (2013).

[45] S. M. Shamid, S. Dhakal, and J. V. Selinger, Phys. Rev. E **87**, 052503 (2013).

[46] *Molecular Fluids*, Les Houches Summer School in Theoretical Physics, 1973, edited by R. Balian and G. Weil (Gordon and Breach, New York, 1976).

[47] J. V. Selinger, Liq. Cryst. Rev. **6**, 129 (2018).
[48] C. W. Oseen, Ark. Mat. Astron. Fys. **A 19**, 1 (1925).
[49] F. C. Frank, Discuss. Faraday Soc. **25**, 19 (1958).
[50] J. Nehring and A. Saupe, J. Chem. Phys. **54**, 337 (1971).
[51] C. Greco and A. Ferrarini, Phys. Rev. Lett. **115**, 147801 (2015).
[52] S. V. Shiyanovskii, P. S. Simonario, and E. G. Virga, Liq. Cryst. **44**, 31 (2017).
[53] C. Meyer and I. Dozov, Soft Matter **12**, 574 (2016).
[54] S. M. Shamid, D. W. Allender, and J. V. Selinger, Phys. Rev. Lett. **113**, 237801 (2014).
[55] E. I. Kats and V. V. Lebedev, JETP Lett. **100**, 110 (2014).
[56] T. H. R. Skyrme, Nucl. Phys. **31**, 556 (1962).
[57] L. D. Faddeev, Quantization of solitons, Princeton preprint IAS-75-QS70, 1975.
[58] N. Manton and P. Sutcliffe, *Topological Solitons* (Cambridge University Press, Cambridge, 2004).
[59] C. Naya and P. Sutcliffe, Phys. Rev. Lett. **121**, 232002 (2018).
[60] J.-S. B. Tai and I. I. Smakyukh, Science **365**, 1449 (2019).
[61] R. Voinescu, J.-S. B. Tai, and I. I. Smalyukh, Phys. Rev. Lett. **125**, 057201 (2020).
[62] D. Foster and D. Harland, Proc. R. Soc. A **468**, 3172 (2012).
[63] E. G. Virga, *Variational Theories for Liquid Crystals* (Chapman & Hall, London, 1994).
[64] J. L. Ericksen, Phys. Fluids **9**, 1205 (1966).
[65] M. Cestari, S. Diez-Berart, D. A. Dunmur, A. Ferrarini, M. R. de la Fuente, D. J. B. Jackson, D. O. Lopez, G. R. Luckhurst, M. A. Perez-Jubindo, R. M. Richardson, J. Salud, B. A. Timimi, and H. Zimmermann, Phys. Rev. E **84**, 031704 (2011).
[66] See Supplemental Material at http://link.aps.org/supplemental/10.1103/PhysRevE.102.042705 for more mathematical details.
[67] http://dlmf.nist.gov/32.
[68] L. Martina, G. I. Martone, and S. Zykov, Acta Appl. Math. **122**, 323 (2012).
[69] G. Baker and P. R. Graves-Morris, *Padé Approximants* (Addison-Wesley, London, 1981).